POLITECNICO DI TORINO

Master's Degree in Nanotechnologies for ICTs

Master's Degree Thesis

Development of electronic instrumentation for a microfluidic microRNA biosensor

Supervisors

Prof. Carlo RICCIARDI

Dr. Pedro G. LOSADA

Dr. Jean GAMBY

Candidate

Martina FREISA

October 2020



This thesis and the information it contains are confidential and intended exclusively for jury members of the master thesis as part of the Master in Nanotechnology for ICTs program.
Any dissemination, publication, total or partial, or disclosure in whatever forms they take are prohibited.

Summary

In this Master Thesis I treat the work that I did during my internship at C2N (Centre des Nanosciences et Nanotechnologies, Palaiseau, France) in the Department of Microsystems and Nanobiofluidics (BioSys team), under the supervision of Doctor Jean Gamby, the Doctor Pedro G. Losada and with the help of the PhD student Claire Poujouly.

The aim of my internship is the development and optimization of an electronic instrumentation for a microfluidic microRNA biosensor. This microfluidic device is a so-called Lab on a Chip and its function is to concentrate, detect and quantify the microRNA from the sample of a patient.

The analysis and quantification of a certain type of microRNA in the plasma of patients give information about their health. In fact, the microRNAs are a particular type of RNA also present outside the cells and so-called circulating microRNAs. Their detection is really effective for medical applications, because different studies demonstrated that their dysregulation might be related to disorders such as cancer, inflammation, cardiovascular or other diseases. These are the reasons why I consider this an interesting and avant-garde project.

This thesis is structured in four main chapters:

- a bibliographic introduction to present the main arguments;
- an explanation of the physics processes exploited by the microfluidic device;
- a chapter for the explanation of the electronic instrumentation and work done by me to improve it;
- a final chapter to introduce the steps for the fabrication of the microfluidic device and the experiments that I done for the electrochemistry detection of the samples.

The first chapter is the state of art of the main techniques for detecting the microRNA and what are their main advantages and disadvantages. In particular, I will highlight the main limitations of the traditional techniques, that cannot be processed in a miniaturizated system such as a microfluidic device.

One of the main advantage of using a Lab on a chip device with respect to traditional techniques for detecting the microRNA stays in its portability, that is why the development of all the electronic instrumentation that makes the sensor working, is important and complex such as the development of the own device.
Furthermore, this type of technology permits the integration of multiple functions in a unique device by increasing the speed of detection, the sensitivity, the throughput and the reduction of costs and reagents.

The device on which I worked exploits different physics phenomena to capture, detect and quantify a certain type of microRNA, these processes are schematically summed up in Figure 2.13.
At first, thanks to the use of nanoparticles, the microRNA under investigation is captured and filtered respect to the other types of circulating microRNA present in the sample (A). Then, thanks to a phenomena called magnetic hypertermia, the microRNA strands previously capture can be deshybridized and therefore released from the nanoparticles (B). Finally, the quantification of the microRNA under investigation is accomplished by exploiting the electrochemical detection (C).
These three phenomena are the heart of this type of investigation, and they will be treated in a detailed way in the second chapter.

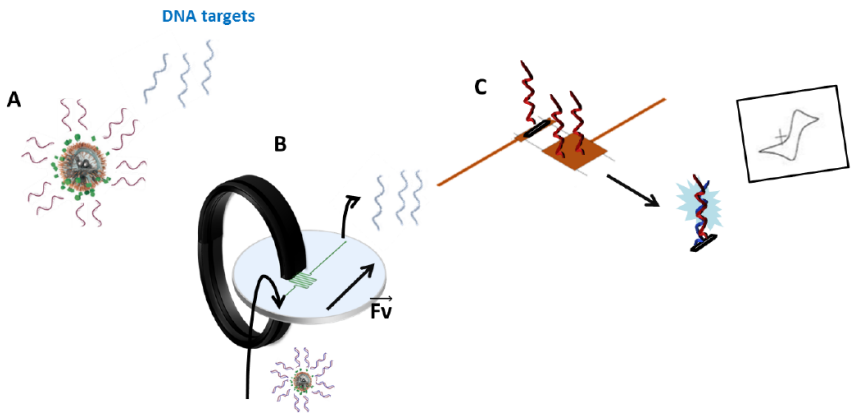

Figure 1: Generic schematics of the three steps in the microfluidic device [1].

In the third chapter, I treat the electronics instrumentation of the device. In particular, I detail the simulation that I did by the use of *LTSpice*, to justify the choice of components used in the board. I reported the characterization done for both the magnetic hypertermia part and the electrochemistry detection part. An then I detail also the improvements that I implemented for both the hardware and software part.

The last chapter is mainly dedicated to the presentation of the experiments that I did to characterize the electrochemical readout electronic. This chapter is

fundamental because I had the opportunity to perform the whole protocol to filter and quantify the sample targets. In this way, the EC board is validated and able to perform the whole electrochemical protocol.

Acknowledgements

I would like to express my sincere gratitude to my supervisors, Dr. Pedro G. Losada and Dr. Jean Gamby , for having accepted me for this internship position and for having always guided me during all the master thesis period.
My thanks goes also to the PhD student Claire Poujouly who helped me in the biological experiments.

Thanks a lot to all the colleagues and friends I met during these years of University. In particular to Chiara, Martina and Marco that supported me from the Bachelor and shared with me the first worries and joys. Federica, my companion of study difficulties and beautiful victories during the Master. Aya for being my favourite colleague during the French M2. My Erasmus companion Giovanna for having shared with me all the adventures in the Gif-sur-Yvette *plateau* and for having taught me almost everything I know about cooking.

I would like to thank also all my friends from the *Canavese*, in particular Laura, Obi, Marta and Cri with who I shared all my athletics training and the best *aperitivi* ever. Lisa and my cousin Paolo who are being always my companion of anxiety, my sweet friend Marta who psychologically supports me and is there by my side from the high school. A huge thank to my boyfriend Davide who always believes in me even when I don't.

Finally I would like to dedicate my thanks to my family: my mum, my dad, my brother and my grandparents; who always personally and economically sustained me and whose support was essential for achieving my goals.

Table of Contents

List of Tables

List of Figures

Chapter 1

Introduction: from the miRNA to the LOC technology

In this introduction chapter I will report the main concepts necessary to understand the experiments and the work that I did and to explain the microfluidic device on which I worked.

At first a general explanation about the RNA will be treated, in order to better know the subject of interest, with particular concentration on the miRNA. It has to be considered that these information are general and not treated from a biological point of view, due to the fact that the main interest in this thesis work is based on a physical and instrumental research.

The microRNAs start being of strong interest when their potential as biomarkers was discovered. For that reason two main bibliographic works are realized: some examples of miRNA biomarkers are reported and a deep analysis of several way of microRNA detection is done.

The last section will be related to the Lab on a chip technology in order to explain how and why a process as the miRNA detection can be integrated. Several aspects of this quite new type of technology will be treated starting from its application, its advantages and disadvantages and concluding with their general fabrication process.

1.1 RNA

The *Ribonucleid Acid* RNA is a macromolecule that, together with the DNA, contribute to guard and transmit the genetic information necessary to the develop and grown of the organism [2, 3].

The nucleid acids, both DNA and RNA, are composed by monomeric units, called nucleotides in which there are three main components[2]:

- a pentose sugar (with 5 carbon atoms) for the DNA is the deoxyribose, for the RNA is the ribose;
- a nitrogenous base or nucleobase;
- a phosphate bridge ($-PO_4^{-3}$).

All these monomeric units are strongly bound each other by a phosphodiester linkage in order to form the single strand. This bond makes polymeric chains to be an anti−parallel, in fact one will start with a $5'$ phosphate and end with a $3'$ free $-OH$ group, while the other one the opposite, that gives to the DNA an inherent polarity [4].
The nucleobases in the DNA molecule can be adenine (A) or guanine (G), that are purine bases containing two aromatic rings, or cytosine (C) or thymine (T) (only in the DNA) or uracil (U) (only in the RNA), that are pyrimidines, containing only one aromatic ring and so smaller.

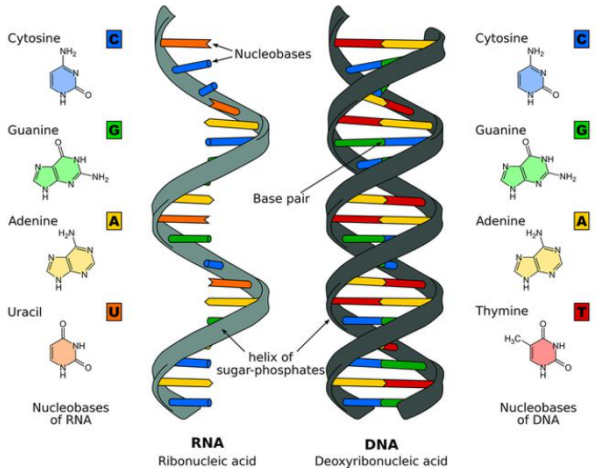

Figure 1.1: Schematic of DNA vs RNA [5].

The RNA is usually formed by a single strand, while the DNA is double stranded, Figure 1.1 represents what explained. For the DNA the two chains are bound together by hydrogen bonds that forms by complementary nitrogenous bases:

adenine can only have a bond with thymine and cytosine with guanine. This means that, when the DNA is analyzed, it would be necessary to discover the sequence of one strand chain because the other one will be complementary. Furthermore, the coupling 'purine + pyramidine' guarantees a constant distance of the two polymers giving it a good stability [2].
The double strand can be *denaturated* and so becomes a single strand when the temperature is enough high such that the hydrogen bonds can be dissolved. However, this is reversible, in fact the single strand can *hybridize* so becomes a double strand, upon some conditions, when the strand are exactly complementary, such that the coupling purine-pyramidine can be guaranteed.

The RNA has a key role for the life, such that some research gives it a main function to lead to the origin of the life on our Planet [6]. However, its main activities were discovered in the last years, in fact, before, the RNA was thought to be only a simple passive messenger that leads information from the DNA to the proteins[7].
It is possible to define the three main types of RNA as follows [8]:

- messenger RNA (mRNA), it codifies the information from the DNA to the proteins;
- ribosomal RNA (rRNA) ; it forms the ribosomes structure and catalyzes the the translation of the mRNA into proteins;
- transfer RNA (tRNA); it is fundamental for the proteins synthesis, it acts between mRNA and amino acids.

These are the three types of RNAs involved in the proteins synthesis. However it was demonstrated also the presence of others RNAs that are not-coding but have significantly others function. For instance, there are the short interfering RNAs (siRNAs) that act as a defence against pathogens, or the microRNAs (miRNAs), that regulate the flux of information in a cell [7].

Even if the quantities of existence RNA types is quite spread, I will explain in detail only the miRNA that is the carrier of information to analyze.

1.1.1 miRNA

The first miRNA was discovered in 1993 in the laboratory of Ambro and Ruvkun, the called it $Lin-4$ [9]. From that year, the research in this field increased exponentially.
The miRNA are non coding RNAs composed by approximately only 20 nucleotides, so quite short compared for instance to a mRNA. They control about the 30% of the coding genome [10]. Their discovery was so important that still nowadays the miRNAs are the subject of thousands of publications per year, in fact their role in

human diseases is still under studies [11].
There are different types of miRNA, nowadays, over 2000 types of miRNA have been discovered in humans [12].
Anyway, the miRNAs have not only the function of regulators, but they also work as intercellular signaling, in fact they are also present outside the cells. They are renominated circulating miRNAs, and they are present in saliva, blood, urine and others bodily fluids [13].

Nowadays the miRNA is still subject of studies, for example some researchers are thinking about using the miRNA as a therapeutic tool [11]. However, by the moment the miRNA has a great potential as a **biomarker** [13].

miRNAs as biomarkers

Multiple researches demonstrated the dysregulation of some circulating miRNAs before or during inflammations, cancers or other diseases [14, 13]. Furthermore, only one miRNA targets hundreds mRNAs, this means that a single miRNA can damage different mRNA and so proteins [15].
Moreover, miRNAs are **stable** (more than mRNAs), provide a **minimal invasivity** and an **early detection** [14], making miRNAs good candidates as biomarkers.
Their stability is guaranteed by the fact that are protected inside the microvesicles, thanks to that, they are resistant to degradation and to different conditions, such as changing in temperature or pH [14]. As already said circulating miRNAs are present in bodily fluids, that's provide a non invasive detection technique and permits the avoiding of tissue biopsy [10, 14]. Finally, in many cases these miRNAs are released during the early development of the disease [10, 14] .

However, their application is not only in absolute quantification of a certain miRNA, but also their profiling. Profiling means measuring the relative amount of a miRNAs cohort among a group of specific interest [16].

Studies reported that the change in the miRNA quantities can be the sign not only of many cancers, such as lung, ovarian, liver, breast, gastric and colon, pancreatic, cervical, and others cancers; but also the sign of bacterial infections (as *Escherichia coli*), different cardiovascular diseases and nervous system disorders, like for instance Alzheimer, epilepsy, Parkinson, and multiple sclerosis [15, 14].

One of the main studies on which the miRNAs demonstrated to be good and valid biomarkers for cancer diagnosis was performed in 2007. Lawrie *et al.* [17] analyzed the serum of 60 patients affected by diffuse large B-cell lymphoma, all the patients were at different stages of the disease. What they found was that high levels of *miRNA21* were associated to a better clinical outcome for the patients. In order to enhance the validity of the *miRNA21* as a biomarker, they compared also the level of that specific miRNA with 43 healthy persons.

The World Health Organization (WHO) states the breast cancer to be the most

frequent cancer among women, and that every year over 2.1 million new cases are found. An early detection can really makes the different between life or death in these cases. Recent studies are based on founding biomarkers for that cancer, and by the moment the *miR-10b*, *miR-196a*, and *miR-4417* sounds to be good candidates [13].

Afterwards, in 2013 other researches demonstrated a link between the amount of four miRNAs : the *miR-499, miR-208b, miR-1* and *miR-133a*, to the myocardial infarction (well known as heart attack) [18].

Moreover, several others miRNAs are biomarkers for many diseases, for instance, the *miR-155* works as a negative regulator during inflammations, or the overexpression of *miR-103a-3p, miR-30b-5p* and *miR-29a-3p* can be linked to the Parkinson [13].

Anyway, the biggest challenge still remains the validity of the link between the dysregulation of miRNA and the diseases. In fact there are some contradictory findings on the circulating miRNAs. For instance, the expression levels can in some cases change depending on age, gender, origin and other individual's characteristic [14, 15]. On the contrary Condrat *et al.* that the miRNAs detection can become a routine approach to develop personalized chart [13].

The aforementioned miRNAs are summarized in table 1.1, in order to give an idea of the spreading of several types of miRNAs as biomarkers for many diseases.

Finally, considering that the cancer and cardiovascular diseases remain the most causes of death in the world [13, 19], and that epilepsy, being the most popular nervous system disorder, affects about the 1% of population, an early detection thanks to miRNAs biomarkers can save or ameliorate lots of lives.

miRNAs	Diseases	Reference
miRNA21	Diffuse large B-cell lymphoma (DLBCL)	[17]
miR-10b, *miR-196a* and *miR-4417*	Breast cancer	[13]
miR-499, miR-208b, miR-1 and *miR-133a*	Myocardial infarction	[18]
miR-103a-3p, miR-155, miR-30b-5p and *miR-29a-3p*	Parkinson	[13]

Table 1.1: Example of promising miRNAs for biomarkers of diseases.

1.2 miRNA detection

Nowadays there are numerous methods for the miRNA detection with different sensitivity, specificity and use. As already said the miRNA detection is fundamental for the diagnosis of several cancers, hepatitis and other diseases, that is why it is a field of huge interest for researchers and medical doctors. In fact an improvement on the miRNA detection would lead to a faster and earlier treatment [20].
In this section I will report the bibliographic work that I made concerning different methods for the miRNA detection.

At first it is important to define the main characteristics that a miRNA detection method should have. It must have an high *sensitivity*: the minimum input parameter that creates a detectable output change, an high sensitivity leads to a more precise detection. Moreover, it must have an high *specificity*: so that the miRNA targets that do not match the detected one do not count in our miRNA quantifying [21]. This point, due to the high homology between different miRNA ,is more difficult and rare to assure [20]. Then, the detection method should be really functional, so must have an high *capability*, in order to guarantee efficiency. It should be easily integrated into a small device, so it is possible a *miniaturization* of its function, finally it should be *rapid*, for having the result in few hours instead of few days.

Now that we know all the main characteristics that our technique should have, it is possible to start by explaining the different methods, starting from the common ones up to the newest and more particular ones. The traditional methods for the miRNA detection are mainly the Northern Blot , the microarray sequencing and real time-PCR (RT-PCR) [22][23][20].
The latter will be explained in the subsection 1.2.1, in order to introduce the methods based on the targets amplification.

The Northern Blot (NB) is based on the separation of the miRNA by gel electrophoresis, from which it is possible to distinguish the target length. Then it is moved and fixed by crosslinking to a membrane where it can hybridize to a complementary radioactive probe. Finally it is visualized [24].
Even if the NB is considered one of the most standard technique for the miRNA detection, it as some disadvantages: in fact it is a slow procedure and require lots of samples and radioactive probes [25].
Alternatively, the microarray consists on a technique on which the samples are immobilized by crosslinking on a self-assembled-monolayer (SAM), such that they can form a microarray. Then the samples can hybridize with fluorescent labeled probes such that, from emission it will be possible to analyze the samples with the relative quantities [25]. This method is really useful for multiples miRNA analysis but not good for absolute quantification [24].
Moreover, the Northern Blotting and the microarray methods have a main limitation: they need a lab (termocyclers and scanners) in order to be realized, this means

that their miniaturization is extremely complicated, if not impossible [22][24].

For these reasons, the overcoming of traditional methods was an important turn. In the following I will present several methods exploited nowadays for the miRNA detection, but at first it is important to understand that the miRNA analysis is based on two main steps: the **amplification** or **isolation** of the target and the **quantification** of it.

1.2.1 Amplification or isolation of RNA or DNA

First of all it is significant to keep in mind that the quantity of miRNA present *in vivo*, such as in plasma or in serum is really low. For example the mean amount of miRNA in stem cells is found to be 0.3 $fmol/10\mu g$ of total RNA [26]. For that reason, in many cases an amplification step is required at first.
In the last 20 years several techniques to amplify the target signal were discovered, due to the increase of the demand in RNA and DNA detection. Anyway, as the title of this subsection suggests, it is possible to distinguish between two methods that assure the amplification of the signal: the *amplification or replication* of the miRNA targets, or the *isolation or concentration* of it. In the first case the miRNA targets are replicated, in the second one, the miRNA targets are concentrated such that the replication of it is not necessary.

Amplification or replication of the targets

The most famous method for the DNA amplification is the Polymerase Chain Reaction (PCR).

The Polymerase Chain Reaction was invetented by Kary Mullins in 1985. The idea is to duplicate a target in several cycles. It takes place in three fundamental steps [4], also represented in Figure 1.2:

- *Denaturation*: the temperature is raised up to 95°C in order to completely separate the two chains of DNA, such that the hydrogen bonds are dissolved.
- *Annealing*: now the temperature is around 40-60°C in order to keep the chains separated and the primers (oligonucleotides) are associated to their complementary sequences. The primers are present in big quantities such that this phase takes around 1 minute.
- *Extension*: the temperature is raised up again to 72°C, during this step the DNA is extended and replicated by the use of an enzyme called *Taq polymerase*.

These three phases are repeated $30-40$ times, and every time the duplicated DNA target become a new sample to be replicated. This means that after n cycles the

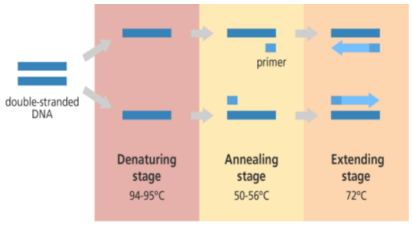

Figure 1.2: PCR phases [27].

chains will be replicated 2^n times, and so that the PCR could amplify a gene by starting from a single cell. This method became really important thanks to its efficiency and speed respect to conventional and older laboratory method [28]. Moreover, it is possible to fabricate microfluidics devices in order to integrate this technique[29].

Anyway, the PCR is not adequate for the microRNA, because it is too short and homologous. In fact, the miRNA contains only 18-22 nucleotides, so a little error can provoke the error in the whole analysis, for that reasons the PCR is inaccurate for it [22].

However, several variants of PCR have been exploited. For instance the so-called Real Time Polymerase Chain Reaction (RT-PCR) is one of these [30]. The RT-PCR is simply figured in Figure 1.3; it uses two dyes both attached to the microRNA to amplify, one is called reporter dye and the other one is a quenching dye. When the extension step of the PCR is occurring, the *Taq Polimerase* will cut the reporter part. By a laser excitation, if both the reporter and quenching dyes are presence (the probe results being intact) the fluorescence emission will be absorbed by the quenching. While after the cleavage, the reporter emission cannot pass anymore to the quenching, so an emission will be detected. As a consequence the fluorescent emission will be proportional to the initial microRNA quantity [31].

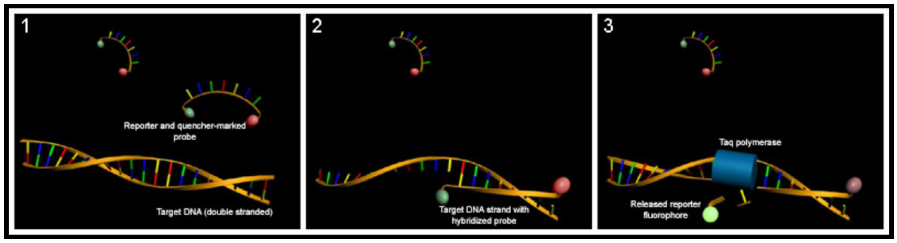

Figure 1.3: Schematic of the procedure of RT-PCR, steps explained in the text [31].

Anyway, this procedure requires lot of time of execution [1] and a device able to easy change the temperature without producing errors in the replication target

[24]. In fact it has to be taken into account that the realization of the temperature cycles it is also a big issue for the realization of an integrated device. For that reason, other techniques are investigated.

The Rolling Cycle Amplification (RCA), for instance could avoid changing in temperature and the use of fluorescent dies. In fact, its main advantage respect to the PCR is the fact that it is isothermal. It differs from PCR by the fact that the double strand is circular, and so the nicking enzyme will start unrolling and replicating the strand [32]. Moreover, it exists other several techniques that are isothermal, such as the two stage exponential amplification reaction (EXPAR), briefly explained in the first example, or the Strand Displacement Amplification (SDA) or the Loop Mediated Isothermal Amplification (LAMP).

However, the requirement of these methods of several and specific primers and templates could cause different errors in the target replication [22]. In fact, in particular the design of miRNAs primers is a crucial point for the sensitivity and specificity [24]. That is the reason why other methods are investigated.

Concentration or isolation of microRNA targets

It is now that the nanotechnology and the nanomaterials come into play. In fact they can be used as special and powerful tools to achieve higher sensitivity, capability and efficiency. Nowadays, RNA techniques differ from the use of nanoparticles (magnetic or not) until the use of the nanotubes.
The nanoparticles are for sure the more exploited means, due to the possibility of utilizing their physical and chemical properties. For instance, some nanobeads have special optical properties that can enhance the signal to analyze. Some others coupled with proteins can capture the target in order to concentrate it in such quantities that the replication of it is not necessary. The same happens by using appropriate magnetic nanoparticles [24].
Also carbon nanotubes (CNTs) have been used for the detection of miRNA, they are suitable for the capture and the immobilization of the ssDNA targets. Moreover, thanks to their properties: heat resistance, hardness and in particular high conductivity, they can provide an enhanced signal [33].

1.2.2 Quantification of the target

After the amplification, the target has to be quantified. The two main possibilities for it are to do it by exploiting optical sensors or electrochemical sensors, these are the most famous, but not the only ones.

In fact, another method to quantify the target is based on Quartz Crystal Microbalance (QCM), it is a mass sensor with a sensitivity beyond ng. The quartz is excited by some electrodes by applying an AC voltage, and due to its

piezoelectricity, it is possible to measure a shift of the fundamental frequency, when there is a variance of mass. The frequency shift will be proportional to the mass variation [34].

Optical sensors (Os)

For what concerns the optical sensors, several techniques are used. For instance, techniques like surface plasmon resonance (SPR) and surface enhanced Raman spectroscopy (SERS) are exploited. The first one is used to measure the variation of the refractive index, since some bio receptors provoke the variation of it when they interact with the target. The last one is based on the quantification of plasmon excitations on metallic nanobeads or nanoroads [14].
Moreover, one of the most used techniques is the fluorescence. Fluorescent labels, in some cases coupled with particular enzymes, are detected, and the intensity will be proportional to the quantities analyzed [35] [36].

Electrochemical sensor (ECs)

The DNA and RNA quantification can carried out thanks to electrochemistry experiments. EC based sensors are really promising due to their precision and efficiency in the signal conversion.

The EC analysis consists on three main steps [37]:

- *immobilization* of the probes on the solid electrodes;
- *hybridization* or recognition with the target to analyze, in order to obtain a double strand system;
- *transduction* or translation of a physical quantity into another that can be easily studied.

This method will be explained more precisely in the following chapter 2.3, in particular, these three steps will be analyzed in details. By the moment, let's simply keep in mind that the transduction is realized when a potential is applied between the electrodes. In fact the targets interact with an electrolyte solution through redox reactions, and so the electrode with the targets. As a result, it is possible to measure a current that is proportional to the quantity of targets.

1.2.3 Some examples

Now that all the main concepts are introduced, I will report some found examples for the whole microRNA detection procedure.

For instance, Y. Zhang and C. Zhang proved an innovative method for the microRNA detection [38]. It is possible to see from Figure 1.4 the stages reported. The amplification (a,b,c) is done by a process called two stage exponential amplification reaction (EXPAR), specialized on the replication of few nucleotides. The advantages of EXPAR are two: it is an isothermal technique and in few minutes provide an amplification of $10^6 - 10^9$ fold.
However, the main innovative part is the detection part that will be done thanks to the use of a quantum dot (QD). The substitution of classical fluorescence methods with this one provides a larger sensitivity and an higher signal to noise ratio. The hybridization provoke the creation of a sandwich hybrid (d) formed by a capture and a reported probe. The capture probe permits the attachment to the quantum dot. The QD excitation is done by an argon laser and the emission is detected by the coupling of avalanche photodiodes with filters. Thanks to the originality and precision of the detection part, the detection limit achieved is 0.1 aM.

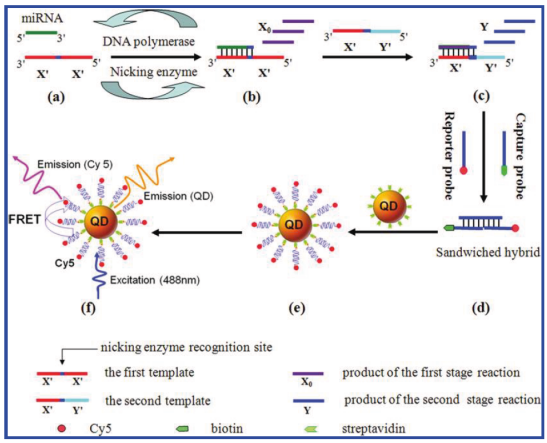

Figure 1.4: Schematic of a *Sensitive Detection of microRNA with Isothermal Amplification and a Single-Quantum-Dot-Based Nanosensor* [38].

Even if the previous technique provides a really high sensitivity, the selectivity for the PCR-based method is still an issue, because of the sample contamination [20].
Furthermore, D. W. Wegman and S. N. Krylov proposed another method whose point of force is the fact that the miRNA is not modify by enzyme reactions[35]. So they developed a method that uses the capillary electrophoresis . As it is possible to see from Figure 1.5, the solution is composed by the microRNAs to be detected, plus their complementary with different fluorescent markers (green circles) and drag tags attached (parachutes). The next step is the hybridization, but some DNA probes will remain single strand. The whole solution is now insert in a electrophoresis section on which also a single strand DNA binding protein (SSB) is

added, such that it can attach the remained ssDNAs probes. In such way, when the electric field is applied, the SSB will make migrate the single probes faster. Finally, thanks to the fluorescent emission, the detection is done at the end of the electrophoresis, and the probes can be distinguished by their migration times.

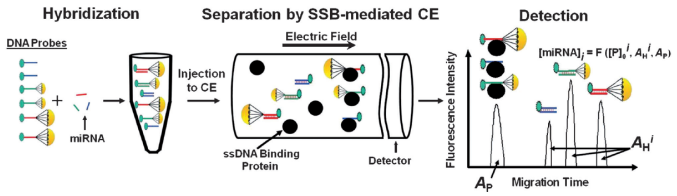

Figure 1.5: Schematic of *Direct Quantitative Analysis of Multiple miRNAs (DQAMmiR)* [35]

However, also this last method has its disadvantages, in fact it requires a specialized equipment, due to the fact that the design of drags tags is crucial for the success of the quantification and it is high time-spending [35].
As already explained, scientists and researcher found another method to quantify the miRNA targets without affecting the selectivity and without requiring specific tags: the concentration of the sample by performing nanostructured tools.

For instance, W.J. Yang *et al*. reported a method based on specific colorimetric analysis by using gold nanoparticles in order to quantify the microRNA [39]. In particular, as showed in Figure 1.6 they used two types of probes: biotinylated probes (brown) on which the microRNAs are attached, and gold nanoparticles (pink) on which their complementary are attached. In such way they can hybridize, and they are immobilized by a plate coated by streptavidin. Then a solution with silver is added. What happens is that the gold nanoparticles catalyze the silver reduction, thanks to that, after soaking, the gray scale is recorded with colorimetric absorbance. The sensitivity of this technique is $10fM$.

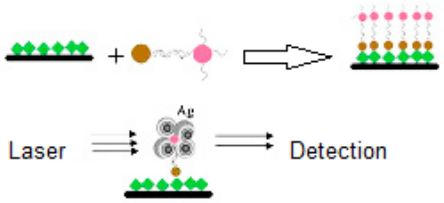

Figure 1.6: Schematic of *Quantification of microRNA by gold nanoparticle probes.* [39]

By another innovative method Capunzanto *et al*. demonstrated that it was possible to detect the miRNA21 by the use of magnetic beads modified by the

use of the p19 protein [40]. In particular, as Figure1.7 shows, from the solution with different types of miRNA, the miRNA21 was recognized, by adding its complementary (labeled with a biotin), such that the hybridization was possible. The hybridized miRNA21s, thanks to their terminal chitin-binding domain, were captured and immobilized by the magnetic beads (chitin functionalized). After, some polymers (Strep-HRT) were added such that they can attach the biotin marker and permit the detection. Finally, the beads were captured by carbon electrodes, such that by electrochemical detection it is possible to estimate the quantity of microRNA with a resolution of 0.04 nM of miRNA21.

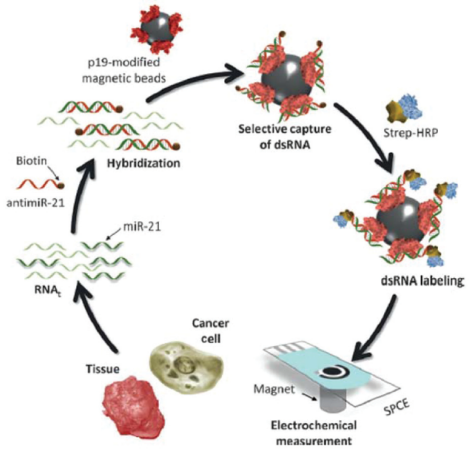

Figure 1.7: Schematic of magnetobiosensors based on p19 modified magnetic beads. [40]

Moreover, Y. Pang *et al.* used magnetic nanoparticles for capturing the miRNA [41]. In particular the nanoparticles are of $Fe_3O_4@Ag$ with a diameter of 400 nm, that assure the immobilization of DNA strands such that the complementary miRNA targets can hybridize. By adding an enzyme which cleaves the double strands without affecting the miRNA, it is possible to recycle the target in order to amplify the signal. Then, the quantification is done by SERS detection. The reached limit of detection of this modality is 0.3 fM.

Finally, it is possible to notice that the variety of methods is really large: there are many different instruments, physical and chemical reactions to exploit and types of target to analyze.
Anyway, we are interested in the precision of the technique in order to overcome detection limits, and to create a microfluidics device able to make an automated detection. For that reason, we have to consider both the limit of detection (LoD) and the integration capability of the method.

From Table 1.2 I summarized the explained examples method with their limit

of detection. It is possible to notice that the first example has the higher LoD, anyway it has to be considered that not biological samples was experimented and that EXPAR produce a nonspecific background amplification [41]. Moreover, it is possible to appreciate that also the high sensitivity by exploiting gold nanoparticles with the optical detection. It can be also noticed that by exploiting the recycling-target amplification (example 5) it is possible to reach a LoD better of 5 orders respect to the concentration of nanoparticles modified by p19 (example 4). However, this comparison is not to consider absolute, due to the fact that in the different methods different types of miRNAs are investigated, and has also to be considered every quantification technique has its own background noise.
To sum up, in general, the concentration of the miRNA targets is mostly used to avoid a low selectivity and both optical and electrochemical quantification assure both sensitivity and selectivity, by avoiding amplification and can be easily miniaturizated [24].

	Amplification	Quantification	LoD
1	EXPAR (PCR-based method)	QD detection	0.1 aM[38]
2	Electrophoresis	Fluorimetric detection	>100 pM[35]
3	Concentration by gold nanobeads	colorimetric analysis	10 fM[39]
4	Concentration by magnetic nanobeads	EC detection	0.04 nM[40]
5	Magnetic nanobeads + target-recycling	SERS detection	0.3 fM[41]

Table 1.2: Comparison between the explained methods and their LoD.

It is possible to understand that recently thanks to nanotechnology, advanced nanomaterials can be exploited, that despite their higher difficulty in processing, they assure biocompatibility, higher precision and they farther guarantee an $in-situ$ detection [22].

1.3 Lab on a chip technology (LOC)

At that point, the idea is to integrate the miRNA technique detection in an unique small microfluidic system, what it is today called **Lab on a chip** (LOC). It consists in an integrated microdevice in which multiple functions are performed, such as a real automated miniaturized laboratory.
The LOC is substantially a mix of fluidics, electronics, biosensors and optics integrated in few square centimeters [42]. In this type of technologies different disciplines converge: starting from physics, chemistry, electrical, mechanical, material engineering and computer science[43].

It finds applications in different fields, such as diagnostic, biotechnology, and medical or pharmaceutic industries [44]; by involving genetic analysis, proteomics, drug revelation and other basic researches [43].
Anyway, the genetic analysis remains the largest involved field, in fact the DNA and RNA analysis are not only interesting for *medicine* and *biotechnology*, but also for *forensic science, agriculture* and *farming*, in order to detect pathogens in food [45], or another curious application can be in *astrobiology* for pathogen and extraterrestrial life detection [46].

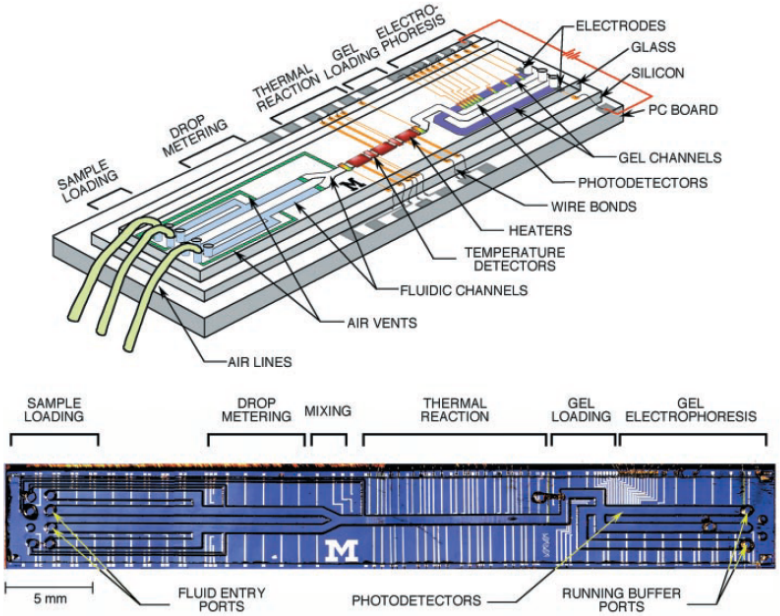

Figure 1.8: Example of a lab on a chip device structure for DNA detection [47].

In Figure 1.8 an example of a Lab on a chip device is reported, its aim is to amplify and detect the DNA and was realized in 1998 [47]. It exploits a drop metering technique, an isothermal DNA amplification (SDA), an electrophoresis

and optical detection technique. From this example it is possible to appreciate how microchannels, microelectrodes, mixers, microvalves, heaters and other sensors can be integrated in a system 47 mm long, 1 mm high and 55 mm wide.

It is possible to intuit that a microfluidic system like a LOC contributes to increase the quantity and the quality of healthcare services in clinical analyses [43]. For that reason, the microfluidics market started been watched from several companies. Just to think in 2013 it was evaluated at $ 1.6 billion, an it was predicted to reach $ 3.6-5.7 in 2018 [48]. From a statistic published in February 2020, in 2019 the microfluidics market was evaluated at $ 13.5 billion, with a estimated compound annual growth rate of 11.3% [49]; and this only without considering the Covid-19 pandemic outbreak.

1.3.1 Advantages and disadvantages of LOC technology

The integration of multiple function in a chip implies several advantages such as the increasing of the **portability**, the **compactness**, the **sensitivity**, the **speed** of diagnosis and treatment and **reducing** the **power consumption** and the **electronic noise**.
The increasing of the speed was a great step forward, in fact, for instance, with standard macro techniques a sequencing protocol requires about $6-8$ hours and costs some hundred dollars, times and money that are not comparable with the LOC technology [45].

Moreover, others important advantages of using a miniaturized system are the **increasing of throughput** due to reduced analysis times and high degree of parallelization [50] the **reduction of reagents and the costs**, that makes the Lab on chip affordable to a larger numbers of individuals.
This last point is not to underestimate, because a cheap device able to do rapid analyses in environments where there are not properly medical equipment can make the difference between life or death to different people living in the third world or countries under development [43]. Just think, for example in Rwanda Chin *et alt.* performed a LOC called mChip to diagnose simultaneously HIV and syphilis [51]. They succeeded in the realization of this test that only need a minimal equipment, only $1\mu L$ of blood, 20 minutes to have the result and it costs only pennies for the material and 10 cents for the reagents.

One of the aim of the LOC devices is to create a system that accomplishes the **point of care (POC)** testing, this means that the diagnostic test are performed near or in some cases by the patient without needing a clinical equipment. For these reasons, a LOC device should be designed as simple as possible for patients who do not receive a technical training [43].

This new concept provides an in loco quick and cheap analysis but has also some disadvantages. In fact the patient has to follow carefully the instruction otherwise

the result can be wrong, then most of lab on a chip requires an external system to work and finally most of this technologies are still not ready and complete for industrialization [52, 27].
Moreover, it has to be considered that almost all the LOCs are single-use, because they are hard to clean and solutions after several usages can degrade some parts (such as electrodes). Finally, their **commercialization** and **standardization** are still an issue [53]; such as the improvement in integration, in fact almost all LOCs require huge external equipment.

Anyway in a nutshell, according to World Health Organization (WHO), the idea device for POC diagnosis should be ASSURED: **Affordable**, **Sensitive**, **Specific**, **User-friendly**, **Rapid** and **Robust**, **Equipment-free**, and **Deliverable** [43].

1.3.2 Miniaturization consequences

It has to be considered that the macro−scale phenomena are not transferred directly to the micro−scale, but several physical properties change. For that reason specialized fabrication processes, design strategies and materials are required and this can present a barrier or an advantage. In fact, when the dimensions are reduced by a factor k, the volume forces, such as mass are reduced by a factor k^3, the surface forces, like pressure, friction or electrostatic are reduced by k^2 and the line forces (ex. surface tension) by k, Figure 1.9 [54, 27]. It also involves an

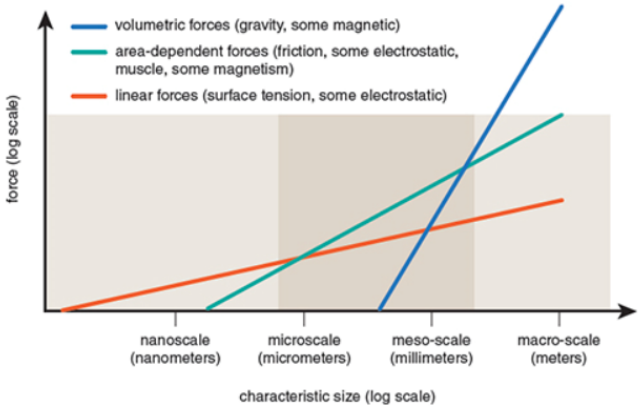

Figure 1.9: Scaling effects consequences. [54]

higher Surface/Volume ratio that requires more attention in controlling the surface characteristic, in fact phenomena like enzyme-wall absorption or sample evaporation are enhanced, affecting the device performances[45]. Another important factor to be controlled is the pressure, it is really important in microfluidic devices, a balance between the needed flow rate and the pressure to be applied has to be found.

Furthermore, in microscopic fluidic systems it is difficult to mix two liquids, this because it is dominated by a laminar flow[27]. In fact when the Reynolds number is less then 2000 the flow has to be considered a microscopic laminar laminar. The Reynolds number is a function of the size and it is expressed as follows:

$$Re = \frac{\rho V D}{\mu}$$

in which ρ is the density, V the characteristic velocity, D the characteristic length or diameter and μ the viscosity.
Finally, in microfluidic devices, in particular in the ones on which processes such as the PCR have to be performed, the temperature control is necessary. For that reason in some cases coolers, heat exchangers and heatsinks can be introduced in order to have a good control of the temperature [55].

1.3.3 Fabrication and materials

As already said, microfluidic devices can integrate microchannels, microelectrodes, mixers, microvalves, heaters and sensors and lots of LOC embody optical and electronics apparatuses [55].
The flow diagram to realize a LOC system is showed in Figure 1.10: the design and prototyping has to be first performed and tested by the use of a numerical simulation. The simulations are important for studying the functionality and the performances of the future device. They consist on finite element algorithms and quasi statically and dynamics analysis [55].

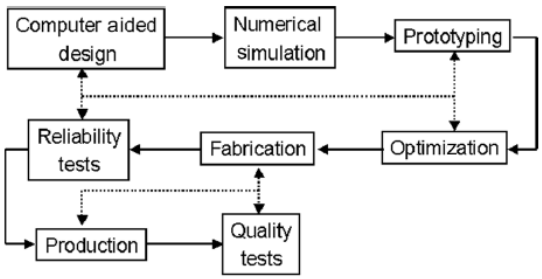

Figure 1.10: Manufacturing process for the realization of a LOC. [55]

The techniques used for the fabrication are the same for the microelectronics devices. The first microfluidic system was made on a Silicon substrate, however, thanks to the advance of technology, modern LOCs combine materials such as glass, polymers (like PDMS) and Silicon.
Polydimethylsiloxane (PDMS) is a polymeric organosilicon compound really used in microfluidic devices due to its flow properties (due to hydrophobicity). Moreover,

it is flexible, non toxic, inert, has a low thermal conductivity and high capability of tight sealing [56].
For what concerns the insulation parts SiO_2, Si_3N_4 and TiN are used, while gold and platinum are used for processing the conductive parts due to their biocompatibility and chemical inert properties.
The procedure for the fabrication is the following one [55]:

- the metallic and insulating layers are deposited on the substrate. In particular chemical vapour deposition (CVD) is used for thin metals and ceramics, plasma enhanced chemical vapour deposition (PECVD)is preferred for insulating films;
- photolithography is used to transfer the pattern for channels valves and other features;
- etching (in most of the cases chemical) for defining the final structures and removing the undesired material. Wet etching is used for the microchannels;
- bonding for sealing the chip. It is done by anodic bonding, thermal bonding , plasma bonding or photopolymer adhesives.

1.4 Chapter conclusions

In the first chapter the main concepts are introduced:

1. At first I defined what is the RNA, one of the most important macromolecules of the organism, responsible to guard and transmit the genetic information. The main differences with the DNA are underlined, in particular concerning their structure.
   Then the microRNA is introduced, a singular type of RNA composed by only approximately 20 nucleotides, with the characteristic of being non coding and to be released in the bodily fluids.
   Their dysregulation can be associated to the presence of different diseases, this, together with their stability, minimal invasivity and an early detection makes them to be good candidate as biomarkers.

2. It has been explained the main methods for the miRNA detection. Starting with the explanation of classical methods such as NB, microarray and PCR, to the newest and most original methods. In particular, it has been underlined how using nanoparticles instead of PCR-based methods can improve the selectivity and the ability of miniaturizing.
   Moreover it has been presented different methods of quantification, mainly based on Os and ECs.
   Finally, several examples are exploited in order to compare their advantages and disadvantages with particular attention to their LoD.

3. In the last part the Lab on a chip technology is treated, it is highlighted the variety of application of this quite new technology, with a special attention to its biomedical role. Then the main advantages of a LOC are remarked , such as their portability, compactness, sensitivity, speed of diagnosis and treatment and the reduction of the costs. Also their role in the POC is stated with a remarking of their potentiality in countries of the third world.
   Finally the main materials , such as the PDMS, and fabrication methods for the microfluidics devices are introduced.

Chapter 2

Physics of the microfluidic device

In this second chapter I will explain in detail the physics processes and the microRNA analysis techniques exploited by the device on which I worked.

Figure 2.1 represents the schematic that sums up the three main steps to realized the detection and quantification of a certain type of miRNA.

1. **Capture**: in the first step the aim is to capture the miRNA to analyze. In order to realize this step, magnetic nanoparticles are employed. In fact, at these nanoparticles will be attached some synthetic nucleid targets complementary to the microRNA under detection. In such way, only the microRNA that we want to analyze will hybridize with its attached complementary target, so that it is possible to easily filter and isolate our target probes.

2. **Release**: the magnetic nanoparticles are inserted in the microfluidic device, there the magnetic hyperthermia step is performed. Thanks to the use of a ferrite with several turns of wire (depicted as black C in the image) a strong alternating magnetic field is generated, causing an increase in the temperature on the nanoparticles and therefore will make release and deshybridize the miRNA targets with their complementary strands.

3. **Electrochemical detection**: this technique is implemented such that it has the double role of filter and quantification. In fact, the microfluidic device will present a two electrodes configuration. At one electrode, the synthetic miRNA strands complementary to the one to analyze are attached, such that, again the miRNAs under detection will hybridize again with their complementary on the microelectrode surface. A redox solution is introduced in the channel, where the electrodes are set, and the voltage is applied between the two

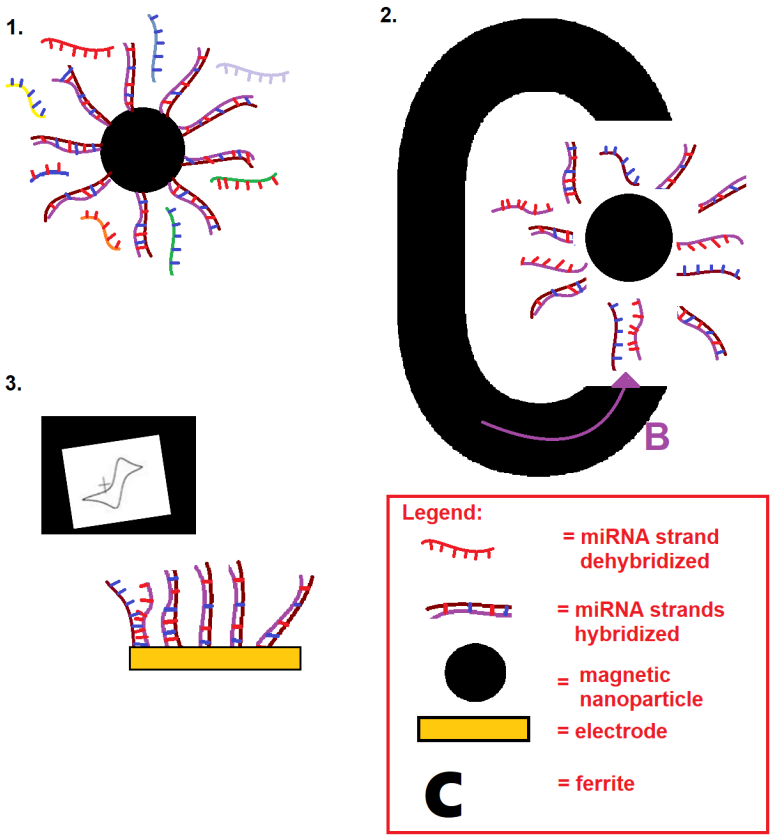

Figure 2.1: Schematic of the three main steps of the microfluidics device: 1. Capture. 2. Release. 3. Electrochemical detection.

electrodes, such that it is possible to obtain a physical quantity to analyze. In particular, by applying a triangular shape potential, it is possible to measure a current, and that current will be proportional to the quantity of miRNAs under investigation.

Every section of this chapter will treat each of the three steps above in order to give more details about the physical phenomena and the device.

2.1 Capture

This first section is devoted to briefly explain the *Capture* step, however, due to the fact that it is a step treated in parallel from another group to which we collaborate to and still in evolution, I will not enter in details.
As already introduced in the previous chapter, nanoparticles and nanobeads are nowadays really used in the field of microfluidics, in fact, they permit to concentrate and select the miRNA to investigate.

The nanoparticles that will be used for this project have a maghemite $\gamma - Fe_2O_3$ core and a SiO_2 shell. The core material is magnetic such that it is possible to perform the hyperthermia process, while the shell material has to permit the attachment of single strand synthetic miRNA on it, the so-called functionalization. In particular the choice of the nanoparticles material is aimed to permit both the easily coupling with biomolecules and the stability after functionalization [1].

In Figure 2.2 the protocol to execute in order to realize this capture step is depicted.

- The bare nanoparticles are first functionalized with synthetic miRNA probes complementary to the specific miRNA that we want to detect. This process is really laborious to realized, because some specific solutions has to be provided for a specific time to the nanoparticles and the binding between the synthetic miRNA and the silica shell will be guarateed by an EDC/NHS coupling [1].

- The sample is introduced, it will contain different type of miRNAs , but only the miRNAs complementary to our synthetic probe will permit the hybridization. Also this step is really delicate , because the miRNA should stay immobilized at the nanoparticles surface.

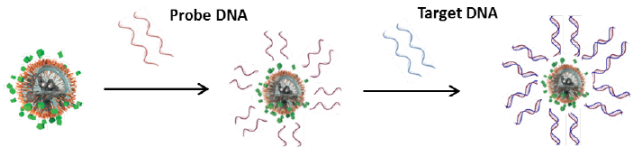

Figure 2.2: Capture protocol by the use of nanoparticles. Image from [1].

At the end of this step we will have the nanoparticles with the sample microRNA to analyze hybridized with its complementary sythentic probe. The next step is the dehybridization and release of the probes.

2.2 Release, magnetic hyperthermia

In this step, the release of the targets and their deshybridization is performed thanks to the use of a physical phenomena called magnetic hyperthermia.

In order to explain how this process takes place, at first the magnetic properties of nanoparticles will be introduced, and then the magnetic hyperthermia phenomena is treated.

2.2.1 Magnetic Nanoparticles (MNPs) properties

Magnetic Nanoparticles (MNPs) are particles with a diameter lower than $1\mu m$, they are composed of a magnetic material such as iron, cobalt or nickel, and they can be manipulated by the use of a magnetic field [57]. They are really used in the field of nanomedicine because they are low invasive and can be biocompatible, for these reasons they are of particular interest for cancer treatments [58].

However, the main advantage of MNPs is in their magnetic properties.
In a bulk magnetic material, the magnetization varies along it, in fact, a magnet contains multiple magnetic domains, so regions where the magnetization has a unique direction, this is shown in Figure 2.3 left.
The domains are separated each one by domain walls, that are interface on which the magnetization changes from one configuration to another.
The creation of a domain is a process dominated by the compromise between the magnetostatic energy and the domain wall energy. So, when the size of the magnetic material reach the order of nm in diameter, it is more energetically convenient having a single domain respect to the creation of a domain wall [58]. For this reason, if the diameter of the nanoparticle is less than a critical diameter that mainly depends on the material, we have a single domain configuration, Figure 2.3 right. This critical diameter is 19 nm for Fe, 74 nm for Co and 10 nm for $FeCo$ [59].

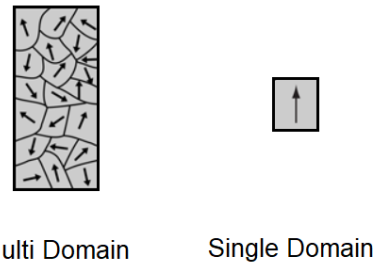

Figure 2.3: Magnetic bulk material, multidomains configuration vs Magnetic nanoparticle, single domain configuration .

In a system composed by magnetic nanoparticles, with the presence of an external magnetic field, the Hamiltonian can be written as the sum of four main contributions:

$$H_{tot} = E_{ani} + E_Z + E_{exc} + E_{dip} \tag{2.1}$$

- the magnetocrystalline anisotropy E_{ani}, that due to the 3D arrangement of atoms in a crystal will tend to lead to a preferred moment orientation;
- the Zeeman interaction E_Z, due to the interaction of the spin intrinsic magnetic moment of the electrons, with the external applied field;
- the exchange interaction or Heisenberg exchange interaction E_{exc}, due to the interaction of two neighbor magnetic moments. If the material is ferromagnetic, the moments will be alligned, with an angle between them of $\phi = 0^o$, if the material is antiferromagnetic $\phi = 180^o$;
- the dipolar interaction E_{dip} that tends to couple all moments together, it is long ranged.

However, by considering a single nanoparticle with an external magnetic field, the two contributions mainly occur: the magnetocrystalline anisotropy energy and the Zeeman interaction, as follows [1, 58] :

$$H_{tot} = E_{ani} + E_Z = K.V.sin^2\theta - \vec{\mu}.\vec{H} \tag{2.2}$$

where K is the uniaxial anisotropic constant, V is the volume of the particle, θ the angle between magnetization and the easy axis, $\vec{\mu}$ the magnetic moment and $\vec{H}$ the external field. If k_BT (where k_B is the Boltzmann constant and T is the temperature) is larger then $K.V$, the nanoparticle is a superparamagnet, this means that the thermal fluctuations are too high to permit a stable order and the magnetic moment changes continuously between two stable states [1, 59].
On the other hand, if $k_BT < K.V$, the particle is ferromagnetic, so its state will be frozen to a stable one.

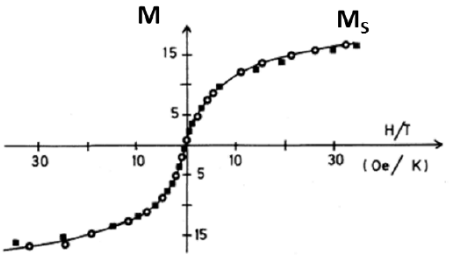

Figure 2.4: Example of a magnetization curve for a MNP [1].

Finally, an interesting thing about the superparamagnetic nanoparticles is that they do not present hysteresis, in fact the magnetization curve, depicted in Figure 2.4, will be described the Langevin function [1]:

$$M = \frac{\mu.\mu_0.H}{k_B T} \tag{2.3}$$

where μ is the magnetic momentum of the single domain particle and μ_0 free space permeability.

2.2.2 Magnetic Hyperthermia

The hyperthermia is technique that consists in body heating, used already more then 5000 years to treat the cancers [60]. In fact in an hyperthermia therapy the cancer cells are damaged by heating the body tissue.

In particular, the hyperthermia is called magnetic when it is caused by magnetic mediators, that release heat by magnetic losses when an AC magnetic field is applied[58].

In our case the magnetic hyperthermia is used to provide enough heat such that the double strands targets deshybridize and leave the nanoparticles.

The heating process of the MNPs by applying an alternative magnetic field is caused by magnetic losses due to hysteresis, Neél and Browian relaxations.

The specific loss power (SLP) is a parameter that describes the heating of the magnet. It is the ratio between the dissipated power and the magnetic mass [61, 1]. It depends on the structure and the material of the magnet, but also on the characteristic of the AC magnetic field applied, such us frequency and amplitude. In order to provoke a good heating the SLP should have an high value.

The magnetic field needed should be high enough to permit the dissipation heat, for instance R. R. Shah *et al.* used a AC magnetic field from 15.1 to 47.7 kA/m (from 188 G to 598 G) to perform the magnetic hyperthermia by the use of iron oxide nanoparticles [62].

2.3 Electrochemical detection

The electrochemical detection, as already introduced in section 1.2.2, is a technique used to perform the quantification of the microRNA (but also RNA and DNA) targets. It is a really simple method that has the advantage of being easily implemented in microfluidics but, in particular, it is a direct measurement, in fact the electrochemistry is a tool to detect electrons transfer [63].

2.3.1 EC detection: Generalities

The representation of a general electrochemical chamber is showed on Figure 2.5.

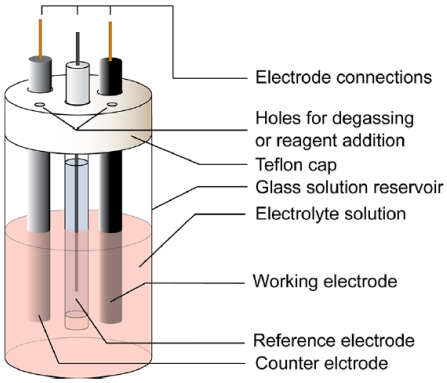

Figure 2.5: Schematic of a general EC chamber, description in the text. [63]

The main ingredients of an EC detection set up are: a *solvent*, a supporting *electrolyte* and the *electrodes* [63], for what concerns electrochemistry sensors for nucleic acid, also a *capture probe* and a *reporter probe* are necessary[64].

The electrodes

The electrodes can be two or three:

- **working electrode (WE)** where the EC reactions accomplish;
- **counter electrode (CE)** to complete the electrical circuit;
- **reference electrode (RE)** used as a reference for monitoring the potential of the other two electrodes, in some particular cases it is avoided.

The choice of the electrodes material plays a fundamental role for the experiment, in fact they must be highly conductive, inert, must have an organized surface for the probe immobilization and must guarantee a large enough potential window

before degradation.
For these reasons, gold is a good candidate for it and one of the most used material for the electrodes, in fact it provides a good adhesion of the nucleic acid, thanks to a streptavidin/biotin binding [1], it is inert and a good conductor. Anyway, the only disadvantage is that it does not provide a large potential window, this means that if the applied potential is too high, the electrodes can easily degrade.
As a consequence, other materials are investigated, such as carbon based materials or platinum, in fact they provide a larger potential windows, but they are less inert. However, the Pt doesn't guarantee a good nucleic acid binding, for this reasons, it can be used combined for instance with the gold, such as counter electrode.

Moreover, also the shape and dimensions of the electrodes are fundamental, because depending on it, the screening of mobile charges will be different [1, 65]. In particular,in the microfluidics scale, in order to assure that the reactions at the WE are not affected by the ones at the CE, the latter is always bigger then the WE [63].

The electrolyte

In this subsection a brief explanation about the electrolyte is provided. The choice of the electrolyte really influences the potential window, moreover, it has to be highly soluble in the solvent, inert and it can easily purified [63]. The solution choice for this experiment is the Ferri/Ferrocyanide that would provide the redox couple Fe^{II}/Fe^{III}.

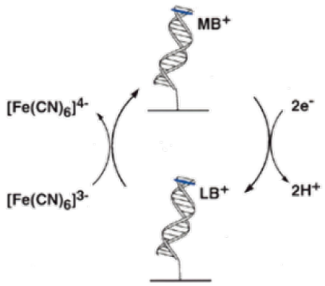

Figure 2.6: Schematic of the Methylene Blue role. It catalyzes the electrolyte solution Fe^{II}/Fe^{III} and permits the electron transfer along the double strand. [37, 1]

Moreover, also a so-called intercalant could be provided, Jiang and Xiang proved that for Cyclic Voltammetry measurements the Methylene blue (MB) is the one that provide the best efficiency [66].
In fact the MB has the double role of redox catalyst and a DNA intercalator, permitting the electron transfer along the DNA as showed in Figure 2.6 [37, 1].

The presence of the MB provides an higher sensitivity of the measurement [1].

Capture and reporter probes

The *reporter probes* (blue in Figure 2.7) are the single strands of microRNA (but also DNA or RNA) under investigation.

The *capture probes* (red in Figure 2.7) are synthetic DNA probes complementary to the ones to analyze. They are in general immobilized at the working electrode and their role is to recognize the reporter probes and to permit them to hybridize.

The hybridization between the capture and reporter probes works as a filter to permit not only the isolation of the probes to analyze, but also the generation of the physical signal under EC reactions.

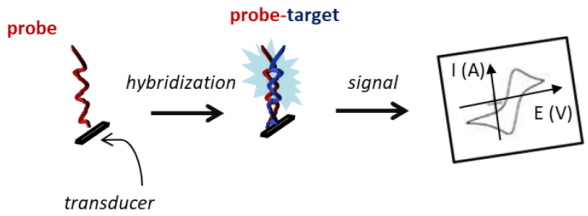

Figure 2.7: Electrochemistry detection : capture probe in red immobilized at the electrode, hybridization between reporter probe (blue) and capture probe, signal generation [1]

2.3.2 Physical and Chemical process

Now that we have all the elements, it is possible to study the physical and chemical processes exploited during the electrochemical measurement.

First of all, it is necessary to distinguish between two types of interactions that occur at the solution-electrode interface[65, 67]:

- Faradaic processes, regarding all the electrons transfer processes, so-called due to the fact that they are governed by the Faraday's law.
- Nonfaradaic processes, that involve phenomena as the movement of ions in the solution, adsorption or desorption and what happens in a current flowing out of the steady state condition.

Faradaic processes

This type of processes describes the charges transfer occurring at the metal solution interface, when a voltage is applied to the electrode.

What happens is depicted in Figure 2.8 [65, 63]. In fact, when a negative voltage is applied at the working electrode, the electron energy at the electrode will raise, such that it can reach the level of the Lowest Unoccupied Molecular Orbital (LUMO) of the solution. In this case, the electron will jump from the working electrode to the solution, causing a reduction of the solution A:

$$A + e^- = A^-. \tag{2.4}$$

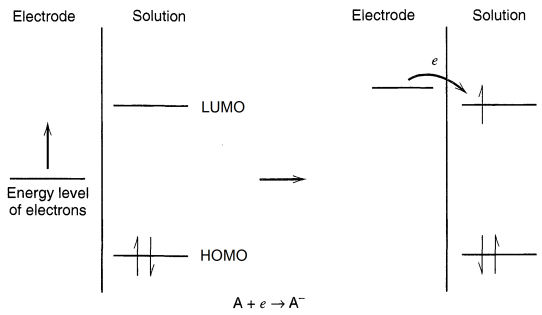

Figure 2.8: Reduction of the solution, by applying a negative voltage at the electrode.

The opposite happens when the applied voltage is enough positive (see Figure 2.9): the energy level of the solution will reach the Highest Occupied Molecular Orbital, such that an electron of the solution can jump into the electrode. In this case we would have an oxidation of the solution A:

$$A - e^- = A^+. \tag{2.5}$$

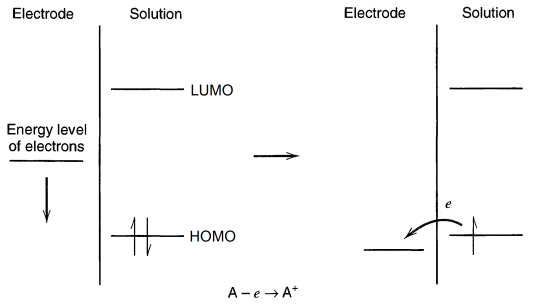

Figure 2.9: Oxidation of the solution, by applying a positive voltage at the electrode.

What happens in the presence of an hybridized target, it is really similar, in fact the redox phoenomena will act along the double strand thanks to the presence

of the intercalant.
In this way it is possible to measure a current, that is proportional to the quantity of hybridized targets, at the working electrode.

Nonfaradaic processes

This type of processes involves the effects of the diffusion and redistribution of the ions in the electrolyte [67, 1]. In fact when a voltage is applied at the electrode, the ions in the solution will redistribute in a more energetically convenient profile, and this induces the creation of a AC current [67].
The solution profile is explained thanks to a double layer model [65], showed in Figure 2.10, it is possible to observe that if the metal electrode is negatively charged the ions will be rearranged such that there will be a first layer or *Inner Helmholtz plane* (IHP) containing positive charges, and a second layer or *Outer Helmholtz plane* (OHP) containing negative charges. This type of arrangement is due to the screening of mobile charges and it is the most energetically convenient for the solution ions.

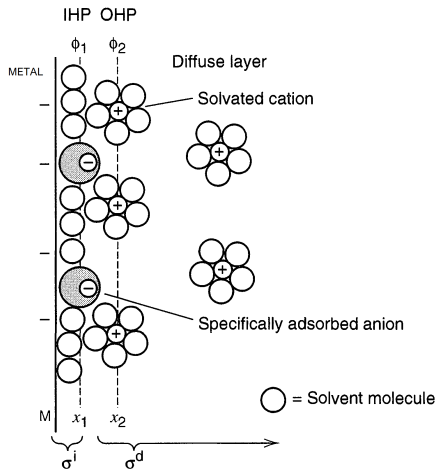

Figure 2.10: Double layer at the electrode-solution interface when a negative potential is applied [65].

Moreover, the region that extends from the OHP into the bulk solution is called diffuse layer. For the conservation of the charge density follows the equation [65]:

$$\sigma_S = \sigma_i + \sigma_d = -\sigma_M \tag{2.6}$$

where σ_S stands for the solution charge density, σ_i for the IHP charge density , σ_d for the diffusion layer charge density and σ_M for the metal charge density.

Faradaic plus Non Faradaic Processes: Equivalent circuit

Randles in 1947 [68] proposed a simple equivalent circuit of what it is happening in an electrochemical cell, represented in Figure 2.11.
First of all, the electrolyte solution is represented by a resistor R_s, at which in parallel are set another resistor (R_{ct}) and a capacitor (C_{db}).
The resistor R_{ct} is related to the charge transfer, so it is the faradaic contribution of the electrons exchange between the solution and the electrode.
The Helmholtz double layers behave like a capacitor, C_{db}, in fact a capacitor is simply composed by two metal layers with a dielectric in the middle. Due to the fact that the ions are mobile charges that reorganize depending on the applied potential, their behaviour is analogue to a dielectric behaviour.

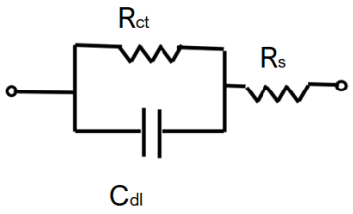

Figure 2.11: Randles equivalent circuit for an electrochemical cell.

2.3.3 Cyclic Voltammetry (CV) measurements

The Cyclic Voltammetry is a type of potential sweep technique very popular for the investigation of the reduction and oxidation processes [63, 65].

A triangular shaped potential signal is imposed between the two electrodes and the current is measured as a function of the potential. The triangular input voltage will be centred in zero, as showed in Figure 2.12a, and a certain scan rate [V/s] is imposed. Moreover, in Figure 2.12b it is represented the current measured as a function of the applied voltage (CV curve) in static conditions. It is possible to observe that there are two main peaks, one for the oxidation and the other one for the reduction.

In fact as explained in the previous section, when the applied potential is enough to reach the LUMO or HOMO level, there is an exchange of electrons that permit the current measurement.
It is also interesting to see the transient current behaviour that will be similar to a capacitive current. Moreover, the current peaks give important information, in

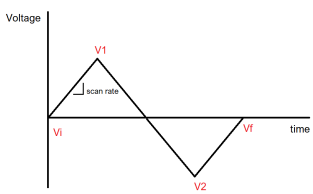

(a) Representation of the input voltage applied between the working electrode and the counter electrode.

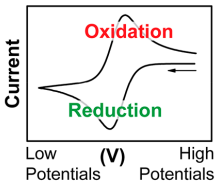

(b) Example of a Cyclic Voltammetry measurement [63], obtained current respect to the input voltage.

Figure 2.12: CV parameters: input signal to send and output signal to measure.

fact as describe from the Randles Sevcik equation [63]:

$$I_{peak} = \frac{n^2 F^2}{4RT} \nu A \Gamma \tag{2.7}$$

where n is the number of exchanged electrons, F the Faraday constant (96 485 $Cmol^{-1}$), R the perfect gas constant (8.3144 $K^{-1}mol^{-1}$), T the temperature, ν the scan rate of the measurement, A the electrode surface area, and Γ the surface coverage of the absorbed species. From this equation, it is interesting to notice the direct proportionality of the peak current with the scan rate, in fact a faster measurement will lead to a smaller diffusion layer [63], due to the fact that the ions do not have enough time to reorganize, and so an higher current.

2.3.4 Advantages of the electrochemical detection

The choice of an EC sensor for the quantification of DNA/RNA is the result of the evaluation of several advantages.

First of all the target quantification by EC detection can be performed in only few minutes, for that reason the **detection speed** that involves the sample recognition, manipulation and the signal analysis has to be considered the first advantage. This advantage, coupled with its **low power consumption** gives to an EC sensor a really high **efficiency** [64].

Moreover, the possibility of integration in a MEMS or in a LOC gives to it all the advantages of these technology; so **economical convenience**,**portability**, **compactness** and the last but not the least the increasing in the **sensitivity**. The archived **sensitivity** for RNA targets is of the order of aM, respect to the several fM for the DNA targets, by considering an amount of sample of several μL. This is guaranteed also because working with small electrodes makes the electric field to be really concentrated, providing a better precision and localization [64].

2.4 Chapter conclusions

In this second chapter the physics phenomena under the device are detailed. In particular it is important to identify the three main part of the system:

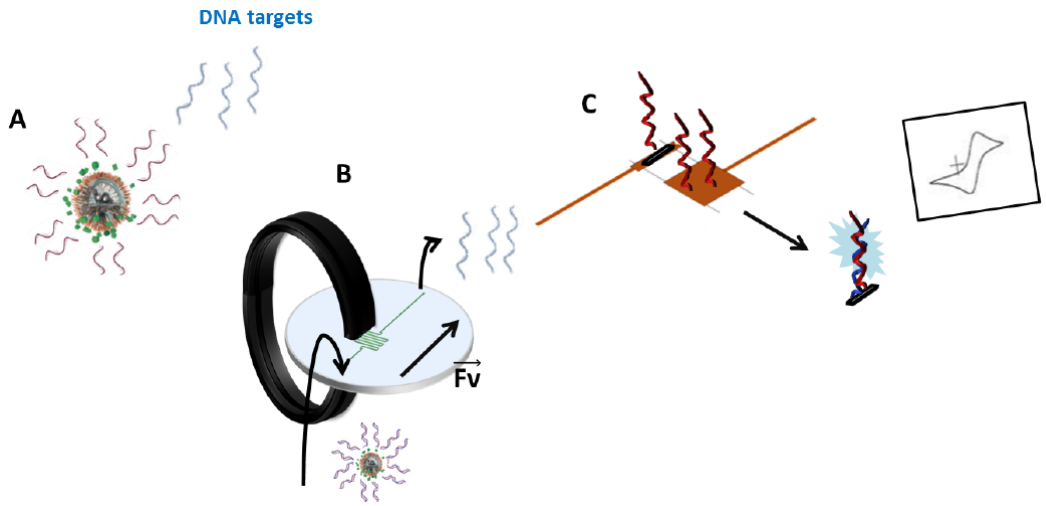

Figure 2.13: Generic schematics of the three steps in the microfluidic device [1].

- A. Capture: that consists on the first stage of our system. Magnetic nanoparticles are functionalized with the complementary target to analyze. This step is still in evolution, however it permits the concentration of the targets at the nanoparticles.
- B. Release : this is the heart of the magnetic hyperthermia process. In fact the deshybridization of the double strand targets and their releasing by the nanoparticles it is possible thanks to an heating. The magnetic hyperthermia protocol takes place: when an AC magnetic field is applied to the magnetic nanoparticle, they will start to present huge magnetic losses that occur in the form of heating.
- C. Electrochemical detection: this is the second objective of the our system. In fact the electrodes are already functionalized with the complementary target to analyze, and the deshybridized targets will arrive from the magnetic hypertermia protocol.
  This step is performed to quantify the microRNA targets. In particular thanks to the applied potential between the two electrode, it is possible to measure the current that will occur at the working electrode and will be proportional to the quantity of microRNA targets in the solution.

This current will occur thanks to two types of processes: the faradaic and non faradaic processes. The first one is due to the exchange of charges due to the redox reactions, and the second one is due to the double layer system forming at the interface between the electrode and the solution.

Chapter 3

Electronic instrumentation

In this chapter I will explain the electronic instrumentation setup to perform both the magnetic hyperthermia and electrochemical steps.

Figure 3.1 represents the whole box containing inside all the elements to perform both the magnetic hyperthermia and the electrochemistry detection. Both the parts are supplied by a voltage supplying board, and they are controlled by a microcontroller. It is possible to observe from the picture also the ferrite that will provide the magnetic field.

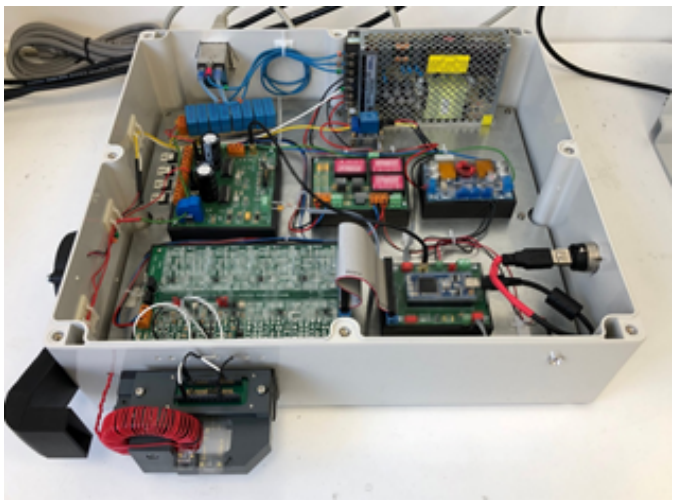

Figure 3.1: Picture of the box containing all the necessary boards to make the full protocol works: hyperthermia part plus electrochemistry detection.

As already explained, for what concerns the hyperthermia process, we need a strong magnetic field to heat the nanoparticles. The AC magnetic field is obtained thanks to the generation of an high AC current ($1 \div 3$A) that will swing by a

conductor wired around the ferrite.
On the other hand, in order to peform the electrochemical measurement to detect the hybridization, a voltage must be applied between the WE and the CE and the circulating current must be measured.
The two electronic equipments are connected to a microcontroller that controls both electronic systems and establish the communication with the user interface. The system is managed by the user thanks to a *LabView* interface.

In the first section I will report the implemented microcontroller program, in order to give a simplified idea of how it works and how to read and send parameters and measurements from the interface.

Then, the magnetic hyperthermia part is explained, with a general explanation of how to generate the magnetic field thanks to the electronics instrumentation, and with a particular attention on the software part so the functions implemented in the microcontroller, to makes the whole protocol working.

Finally, the electrochemical instrumentation is treated, in particular the general circuit setup is explained, with particular interest in the part regarding how to measure the current at the working electrode. Some simulations that I did are also reported, in order to study the behaviour and the components of the circuit that assure a good signal to read, then the simulations are compared with the experimental results, thanks to the characterizations done. Finally, for the software part, a function that I implemented in the microcontroller code is explained and also a *MATLAB* code implemented for the data analysis is treated.

3.1 Microcontroller program and Lab view interface

As already discussed, the microcontroller is responsible of managing the electronic subsystems that generate the current for the magnetic hyperthermia and perform the electrochemical measurement.

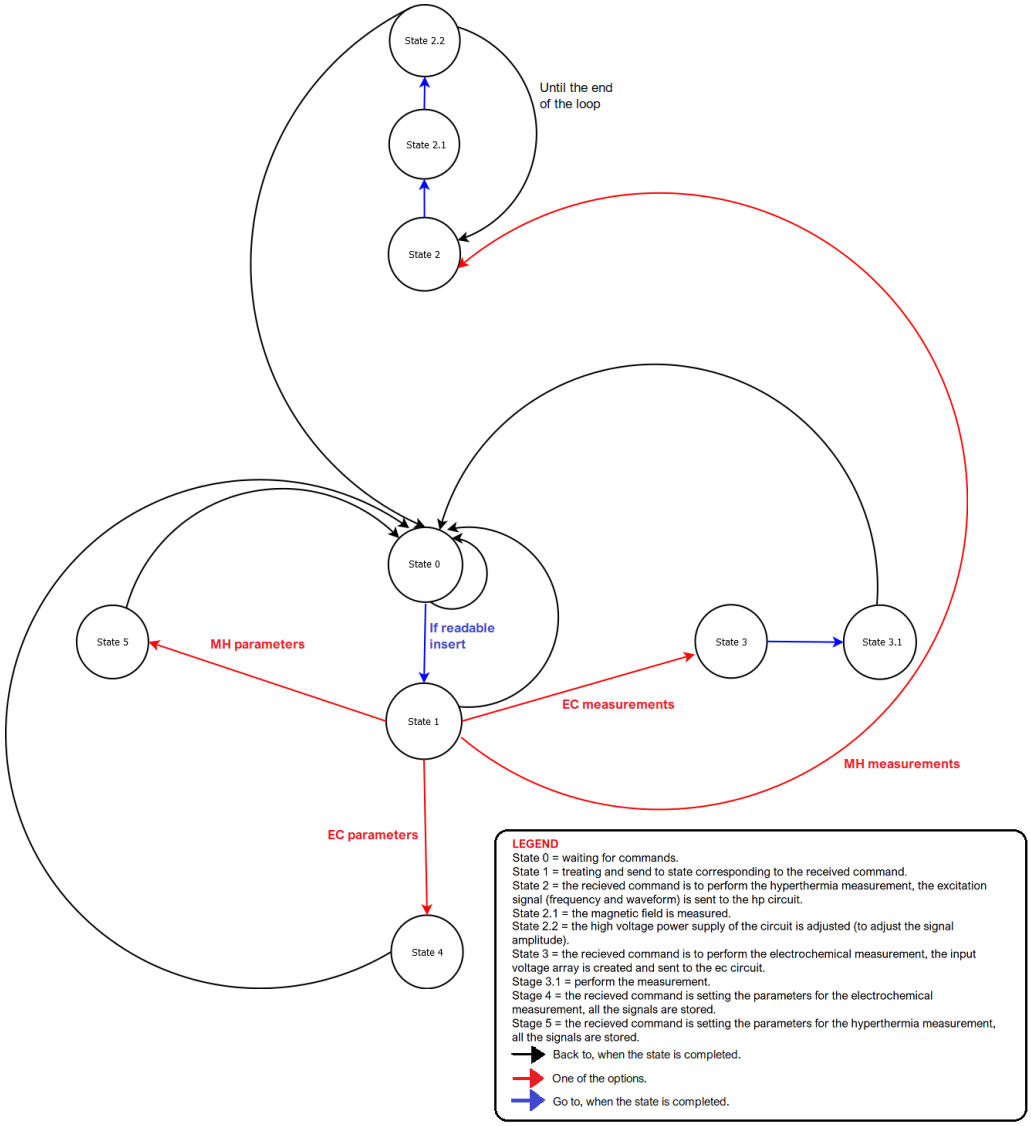

Figure 3.2: Diagram of the microcontroller code with legend.

Figure 3.2 represents the diagram of the microcontroller code. It is possible to

observe the functions that can be performed are mainly four:

- set the parameters for the electrochemical detection;
- set the parameters for the magnetic hyperthermia;
- perform the electrochemical detection measurements;
- perform the magnetic hypertermia measurements.

One of these commands is read by the state 1 and the following state will be the selected command.

If the selected command is *set magnetic hyperthermia parameters* the following parameters are sent:

- the frequency in kHz to center a span for finding the resonance frequency of the system;
- the span of frequency where to find the resonance frequency;
- the duration time in seconds to perform the magnetic hyperthermia protocol;
- the voltage to supply to the electronic system.

If from state 1 the selected command is *set the parameters for the electrochemical detection* it is moved to the state 4, on which the information are saved. The setting parameters are:

- the initial voltage value V_i, from Figure 3.3a;
- the final voltage value V_f, from Figure 3.3a;
- the intermediate voltage value V_1, from Figure 3.3a;
- the intermediate voltage value V_2, from Figure 3.3a;
- the scan rate, so the slope of the triangular signal (V/s);
- the number of samples, so the number of measurements during a period;
- the channel selected (the platform has 8 channel, this means that 8 measurements can be performed par time);
- the number of cycles;
- the number of samples par point, so how many measurements are taken for each point;

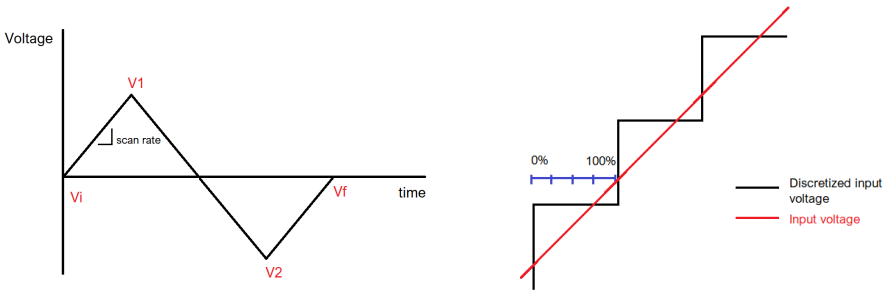

(a) Input voltage sent to the CE in order to perform the Cyclic Voltammetry measurements.

(b) The integration time is referred the point of the discretized sent signal at which the measurement is taken.

Figure 3.3: Images regarding the input signal to send to the CE. Some input parameters are represented.

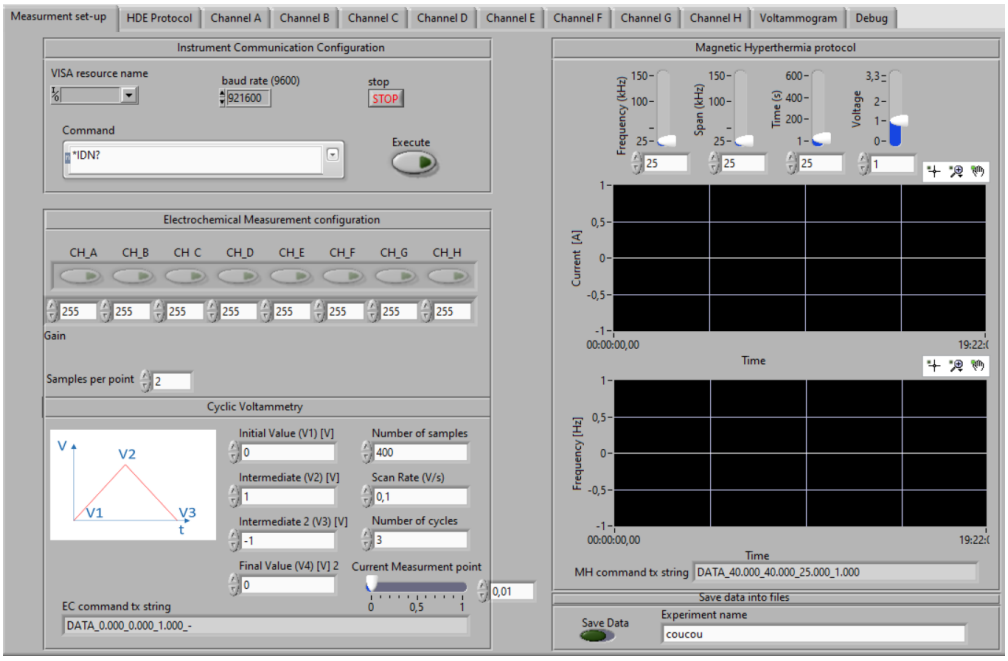

Figure 3.4: LabView interface, it is possible to identify the two windows, one for the hyperthermia parameters and the other one for the electrochemistry parameters.

- the code gain of the potentiometer (explained after);
- the integration time in percentage for each voltage value sent, represented in Figure 3.3b

In the Appendix A, it is possible to find a short review of some parameters to show their influence in the measurement. Figure 3.4 shows the LabView interface

where to configure all the parameters explained above, it is possible to identify that the left side is to set the electrochemical parameters described above, while the right side for the hyperthermia parameters.

Then, if the selected command is to *perform the magnetic hyperthermia measurements*, at first the resonance frequency of the system is find, and then the protocol is performed for the time inserted.

Finally, if the selected command is to *perform the electrochemical measurements*, the input voltage is sent to the CE thanks to the circuit explained in the following section. The collected current at the WE is plotted in two different figures: respect to the time and respect to the applied voltage, as shown in Figure 3.5.
It is also possible to visualize the applied polarization voltage.

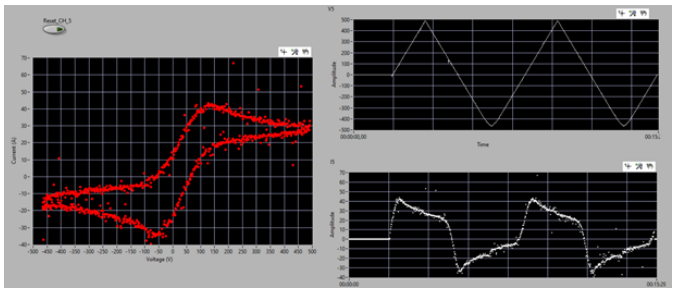

Figure 3.5: Example of an EC measurement: the current is plot respect to the input voltage (left), the input voltage respect to the time (right top), the current respect to the time.

To conclude, another possibility is added in the commands, that stays for "*Perform the full protocol*", on which the Full protocol: magnetic hyperthermia plus electrochemical detection, can be performed. It is not mentioned in Figure 3.2, because this state (state 6) was added at the end, but a section will be dedicated to it.

3.2 Magnetic hyperthermia instrumentation

In this section, the magnetic hyperthermia instrumentation is explained. As introduced before (chapter 2.2), the aim is to heat the nanoparticles such that they can release and let the DNA targets deshybridize. For realising this step, an high magnetic field is needed, such that the magnetic hypertermia phenomena can occur.
The magnetic field can be created thanks to the use of an inductance, as showed in Figure 3.6. In fact a number N of coils turning along a magnetic material, such as a ferrite, create an alternating magnetic field when an AC current is provided to the coils. The magnetic field will be as follows:

$$B = \frac{\mu_0 N I}{l} \tag{3.1}$$

where μ_0 is the permeability constant, N the number of coils, I is the current and l the gap length. The gap is created in order to insert the microfluidics device inside it.

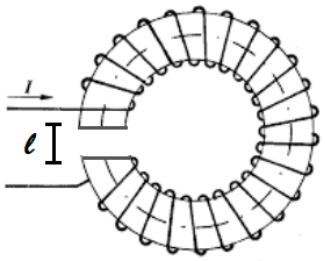

Figure 3.6: Inductance with a gap length l.

In series to this inductance is inserted a capacitor, as a consequence we will have a resonance LC circuit (Figure 3.7a).
The total impedance of the LC circuit is composed by the impedance of the inductance in series with the impedance of the capacitor and, since both impedance are frequency dependent, the resulting impedance depends on the frequency as shown as follows:

$$Z(j\omega) = Z_L + Z_C = j\omega L + \frac{1}{j\omega C} \tag{3.2}$$

as represented in Figure 3.7b, the sum of these two contributions leads to a resonance frequency, on which the impedance will be minimum, so a maximum current. This resonance frequency will be equal to:

$$f_0 = \frac{1}{2\pi\sqrt{LC}}. \tag{3.3}$$

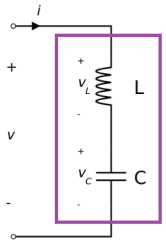

(a) Schematic of an LC circuit. Image from [69].

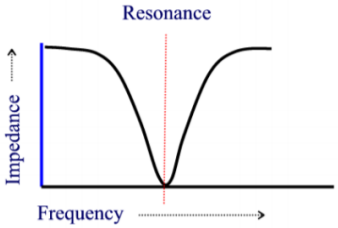

(b) Impedance respect to frequency according to equation 3.3. Image from [70].

Figure 3.7: LC circuit characteristics.

The aim is to provide enough current to the magnetic circuit to generate the required magnetic field that will heat the nanoparticles, for that reason it is convenient to work at the resonant frequency . This is done by exciting with a so-called H-bridge, the resonant circuit formed by the magnetic circuit and the series capacitor at its resonant frequency where the impedance is the lowest and therefore the transmitted current will be maximized.

Moreover this current is generated by an appropriate circuit, whose block schematic is showed in Figure 3.8.

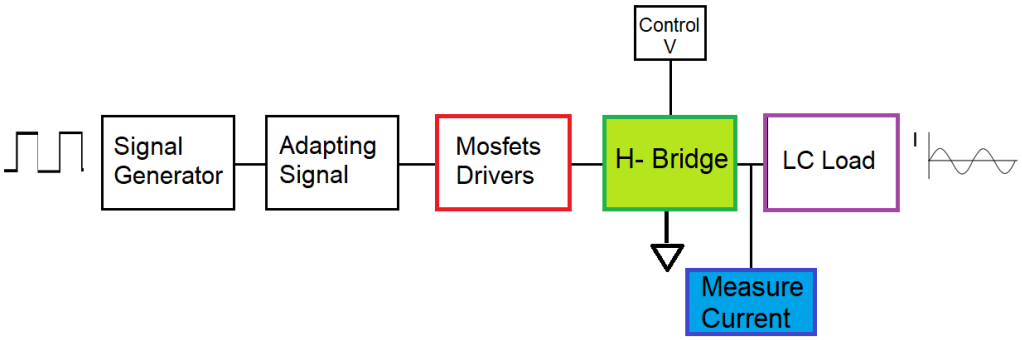

Figure 3.8: Schematic of the magnetic hyperthermia electronics set up.

In the first step (Signal Generator block), a squared wave voltage signal is generated by the microcontroller.
In the second block this signal is adapted to reach the MOSFETs drivers. In fact, it is firstly amplified by a non inverting amplifier and then thanks to the use of a pulse transformer with two outputs it is duplicated (A and B) and one signal is shifted of 180^o respect to the other. This double polarity is necessary to the generation of the AC current, as we will see in the next step. The transformer

provides also a galvanic isolation to the circuit.

The third and fourth block are represented by the two MOSFETs drivers and the H-bridge respectively. However, these two parts are represented in Figure 3.9 in order to give a more detailed idea of how they work.

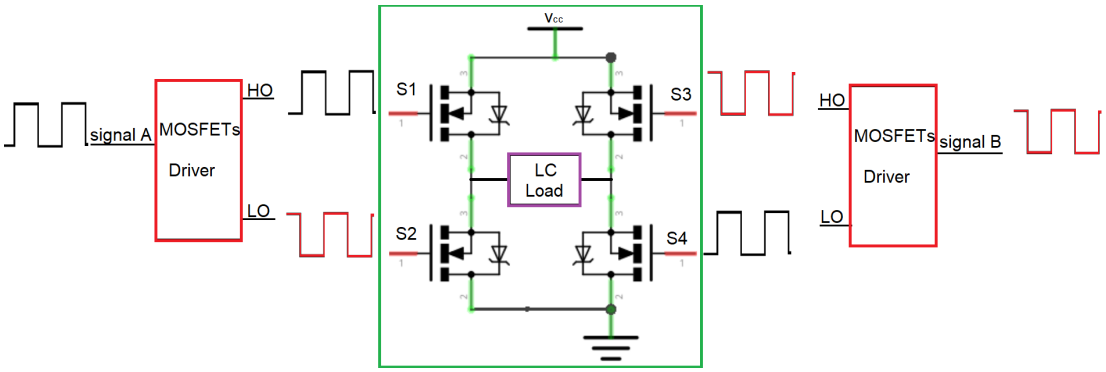

Figure 3.9: Detailed representation of the MOSFETs drivers and the H-bridge.

In one driver enters the signal A and in the other, the signal B shifted of 180^o. Each driver has two output: a low output and an high output, and one signal is shifted respect to the other of 180^o. This means that at the end we will have that the low output of the driver one will be equal the high output of the driver two, and the high output of the driver one will be equal to the low output of the driver two.

Then, there is the generation of the AC current: this is possible by using an H-bridge (or full bridge).

An H-bridge is a circuit composed by four MOSFETs, as represented in Figure 3.9, the switch 1 (S1) commutes with the switch 4 (S4) and the switch 2 (S2) with the switch 3 (S3), as it is possible to see in the figure. This means that when S1 and S4 are closed, a current will flow from the power supply V_{CC} to the ground, passing in one sense through the load. On the other hand, when S2 and S3 are closed, the current will flow through the load in the other direction. This will generate an AC current that flows in our load.

The amplitude of this current will depend on the voltage supply V_{CC}, this voltage is provided by a dc-dc converter controlled by the microcontroller and it is the selected voltage by the user from the interface. This is a really important point because with the V_{CC} it is possible to decide the magnetic field to create directly from the interface. In Figure3.8 this step is represented by the block Control Voltage.

Finally, it is important to know in every moment the amount of magnetic field applied to the nanoparticles. This magnetic field will be proportional to the AC current generated, in fact this step is represented from image 3.8 as Measure current

block, but in order to enter more in details a schematic for this block is shown in Figure 3.10.

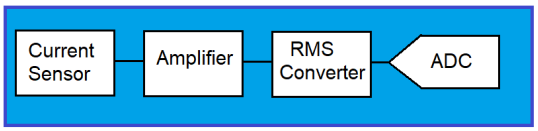

Figure 3.10: Detailed block representation of the block "Measure I" in Figure 3.8.

First of all, the wire that will wrap the ferrite will first pass through a current sensor. This current transducer, by exploiting the Hall effect, will provide a voltage output proportional to the current that crosses the wire. In particular:

$$V_{out} = 2.5 \pm \left(0.625 \frac{I_{in}}{I_{PN}}\right) \tag{3.4}$$

where I_{in} is the current that we want to measure and I_{PN} is equal to $6At$.
Then, the second step is the amplification of this V_{out}, this is done by the use of an Instrumentation Amplifier, and the signal, that at the output of the current transducer is also shifted of 2.5 V, it is now shifted again of - 2.5V. The gain of the instrumentation amplifier will be as follows:

$$G = 1 + \frac{6k\Omega}{R_G} \tag{3.5}$$

where R_G is equal to $1k\Omega$.
Finally, thanks to a RMS to DC converter, the AC voltage is converted to a DC signal having its RMS value, as follows:

$$V_{out} = \frac{V_{PP}}{\sqrt{2}} \tag{3.6}$$

where V_{PP} is the peak to peak input voltage. Finally this value is sent to the microcontroller and can be read from the interface by an appropriate function in the code.

To sum up, the total gain will be as follows:

$$G_{tot} = G_{sensor} * G_{amplifier} * G_{RMS} = \frac{0.625}{I_{PN}} * \left(1 + \frac{6k\Omega}{R_G}\right) * \frac{1}{\sqrt{2}} \tag{3.7}$$

3.2.1 Relation between the current measured and the magnetic field

From the previous explanation, it is possible to understand that the use of a current sensor, with its conditioning circuit, allows the user to visualize the level of current delivered to the magnetic circuit in real time.

However, the user will be more interested in having the measure of the magnetic field instead of a voltage, that is why, by characterizing every component with the oscilloscope I found the experimental gain for the amplifier gain plus the RMS converter gain for reading the current, that corresponds to 3.8 instead of 4.95.

Now, it is possible to experimentally find the relation between the magnetic field and the current read. In fact, thanks to the use of a wire loop where a voltage is induced by the magnetic field and connected to an oscilloscope, it is possible to measure the voltage in the middle of the gap magnet. Then, it will possible to find the peak to peak AC magnetic field by using the following formula:

$$B = \frac{V_{PP}}{2(\pi r)^2 f} \tag{3.8}$$

where V_{PP} represents the peak to peak voltage read at the oscilloscope, r represents the radius of the loop you put inside the ferrite and f is the working frequency. The formula used is the one exploited for our ferrite configuration (material, size and geometry, wire, number of turns).

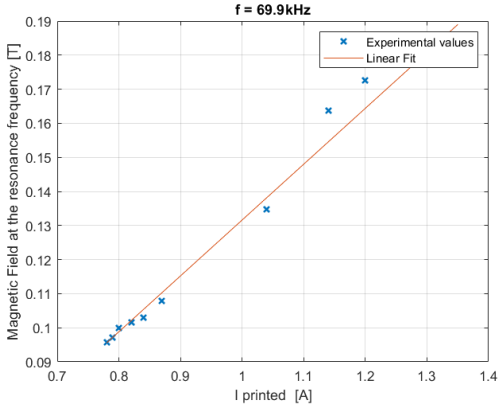

Figure 3.11: Magnetic field measured by the oscilloscope respect to current measured by the electronics.

This measurement is done by changing the voltage supply of the H bridge by the interface.

In this way, the print current plotted respect to the magnetic field measured by the oscilloscope and the results are plotted on Figure 3.11. A linear interpolation is done with Matlab and the slope find is 0.1639 T/A, while the intercept is -0.0323 T.

3.2.2 Function implemented in the microcontroller code

Now that all the electronics instruments behind the magnetic hyperthermia part are explained, I will treat the function implemented to perform the hypertermia protocol.

Resonance Frequency

As explained in the previous section, we need an high magnetic field to heat the nanoparticles, so it is opportune to work at the resonance frequency of the LC circuit composed by the inductance (ferrite with turns) and the capacitance. In fact in this way, it would provide the lowest impedance and so the highest current (and highest magnetic field). For that reason, the aim of the first function implemented in the microcontroller code is to find the resonance frequency.

In order to do it, the user will provide a frequency to the interface, as showed in Figure 3.4 and a span where to center the frequency sweep. So, when the user, after setting these parameters, will perform the MH protocol, this function will be called first.

For evaluating correctly the resonance frequency, it is important to work at low voltage supply to avoid the noise due to very high voltage peaks on the inductance turns, for this reasons in this part, the voltage insert by the user will not be taken into account. This evaluation will be done by keeping the voltage at ≈ 18 V.
Once that voltage will be supplied to the H-bridge, the signals A and B depicted in figure 3.9 that will be provided to the bridge, will be swept in frequency.
In fact, the frequency is swept between $\left[f_{insert} - \frac{f_{span}}{2} \div f_{insert} + \frac{f_{span}}{2}\right]$ by changing the frequency with a step of 0.5 kHz. In the meanwhile the current is measured (block depicted in Figure 3.10), and plotted to the interface.
In order to reduce noise, the current plotted will be averaged between 20 samples, and by passing from a frequency and the other $200ms$ are waited, such that the current can adjust.
When the value of $f_{insert} + \frac{f_{span}}{2}$ is reached, the maximum current is evaluated, such that in the next cycle the span will be centered at the frequency corresponding to the maximum current, so almost the resonant frequency. The same procedure is done, but for this second cycle, the step is 0.1 kHz, in order to improve the accuracy of the resonant frequency.
Again the current is calculated for each value of frequency, and the maximum current will correspond to the resonant frequency.
In Figure 3.12 the results by the interface in real time are shown, it is possible to clearly define the two cycles, and to identify the maximum current that will correspond to the resonant frequency. In fact, the measured current respect to the time is plotted, the parameters insert for this example are 70kHz for the

frequency where to center the span of 50kHz over which the program will look for the resonant frequency. In this case the resonant frequency found is at 69.49kHz. The hyperthermia protocol now can take place, so the found resonant frequency

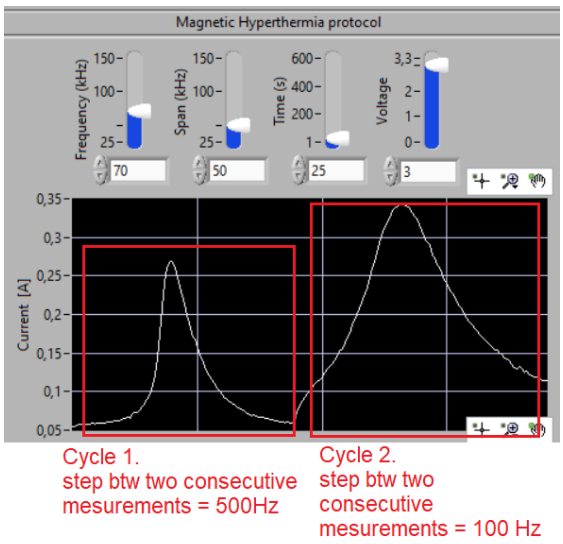

Figure 3.12: Current respect to time during the process of finding the resonant frequency.

and the voltage insert by the user are set, the protocol will last for the time in seconds sent by the user.

Finally, for the second cycle, the current is plotted respect to the frequency, in Figure 3.13 it is possible to see an example, when the span is equal to 80 kHz, in this way, it is possible to appreciate the whole profile of the current - frequency graph.

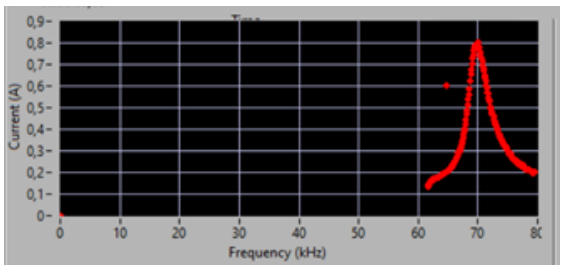

Figure 3.13: Current respect to frequency during the last cycle.

Tracking the resonance frequency

When the hyperthermia protocol is performed, the heat dissipation in the ferrite makes the resonance frequency shift to higher frequency. For that reason, at a certain time the load current will decrease if the frequency will be kept constant. That is why, I implemented a function in the microcontroller able to adjust in an automated way the frequency at which working, when the level of current starts being low, and so also the magnetic field generated decreases.

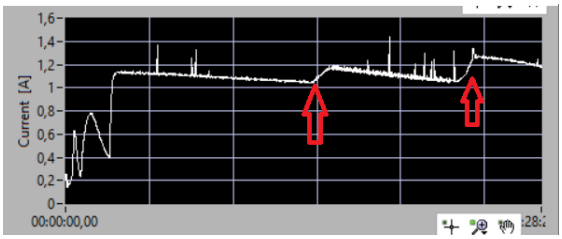

Figure 3.14: Labview interface for the function to find the resonance frequency plus track it during the protocol, the red arrows highlight when the current starts being less then the threshold current established, so the new resonant frequency is found.

The aim of this function, so it is the tracking of the resonance frequency during the magnetic hyperthermia performance. In Figure 3.14 it is possible to see that after the two cycles to find the resonance frequency, the frequency is set to that frequency, as a consequence, the current really increases fast.
What this function does is that, when the current starting stabilizing, a threshold is established. In fact after around 70 points (enough for the stabilization of the current), the current value is stored and at that value is subtracted the experimental value of 0.05 A, (which corresponds to 0.084 T for the current magnetic circuit configuration), this will be the threshold.

In this way, if the current will reach this threshold value, the frequency will sweep with a span of 3kHz starting from the value of the previous resonant frequency minus 500Hz, by a step of 50 Hz. As in the function explained above, the maximum current is evaluated and the frequency corresponding to the maximum current will be the new resonance frequency.

In Figure 3.14 it is possible to observe this function working, in fact, after a certain time it is possible to see the current decreasing, and thanks to the swept of the frequency, the new resonant one is found, such that the current will increase again. In the image this mechanism is performed twice (red arrows).

3.3 Electrochemical instrumentation

In this section the electronics instrumentation necessary for the electrochemical detection is explained in details, furthermore also some simulation to justify the choice of the components are reported. The laboratory instrument that performs this type of measurements is called potentiostat, there are different types with different functionalities, the aim is to implement a portable, multiplexed and low cost potentiostat able to perform electrochemical analysis in the simplest way.

As explained in the previous chapter, a polarization voltage has to be applied between the working electrode and the counter electrode, in order to let the electrochemical reaction takes place. In fact, when a potential difference is applied , the REDOX reactions between the solution, electrode surface, and DNA targets will create a current that can be collected at the working electrode. This current is the figure of merit necessary to quantify the interesting targets of our sample.
For that reason is clear that the potentiostat is composed by two main parts [67]:

- the voltage generation circuit, connected to the counter electrode;
- the current reading part, connected to the working electrode.

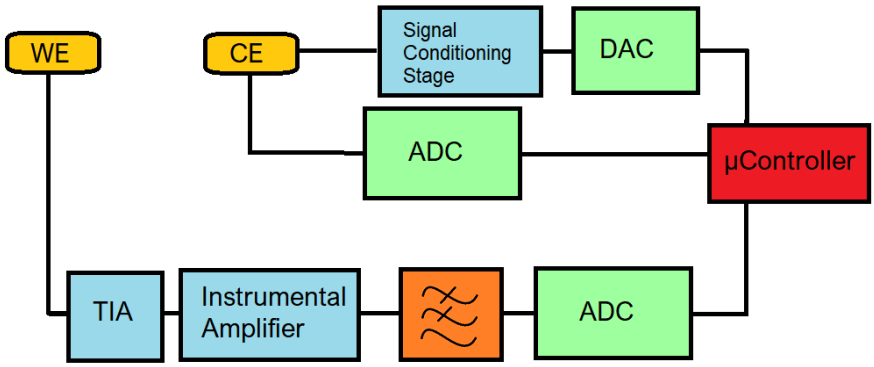

Figure 3.15: Electronic schematic for the electrochemical instrumentation.

In Figure 3.15 is represented the electronics schematic implemented. Both the working electrode (WE) and the counter electrode (CE) are represented in yellow. The CE is polarized by an input voltage signal thanks to the microcontroller (red), but this signal is firstly converted into an analog one, thanks to a Digital-to-Analog-Converter (DAC, green). Then, thanks to a signal conditioning stage, it is amplified, adjusted and a following amplifier ensures the stability of the polarization voltage (light blue). In order to further check that the input voltage signal is the one

expected, the CE is also connected to a Analog-to-Digital-Converter (green) that allows the system to sample the actual applied voltage and sends it to the interface. In such way the voltage is generated between the CE and the WE.

On the other hand, the collected output current at the working electrode has to be measured as a function of the input voltage in order to obtain the Cyclic Voltammetry (CV) measurement. However, this current signal is on the order of nA, for that reason, before converting the signal into a digital signal, it has to be amplified. Moreover it is also necessary to transform it into a voltage, in order to be read by the converter.
This step is done by converting the current into an higher voltage signal, thanks to the use of a transimpedance amplifier (TIA, light blue), then the signal is further amplified by the use of an intrumentation amplifier (light blue), in fact it adequates the signal converted by the TIA to the dynamic range of the ADC.

However, all these amplification stages will amplifly also the noise, for these reasons some low pass filters are added to the circuit, one is after the TIA stage, even if not represented into the schematics, and the last one is represented as the orange block after the instrumentation amplifier stage. Finally, the amplified, filtered voltage signal is converted into a digital signal, by the use of an Analog-To-Digital-converter (ADC, green block) in order to be read from the microcontroller.

In Figure 3.16 is represented the used board in order to perform multiple measurements at the same time. It is possible to notice the presence of 8 channels, this means that 8 measurements at the same time will be possible, in fact each of the channel will contain the components explained in Figure 3.15.

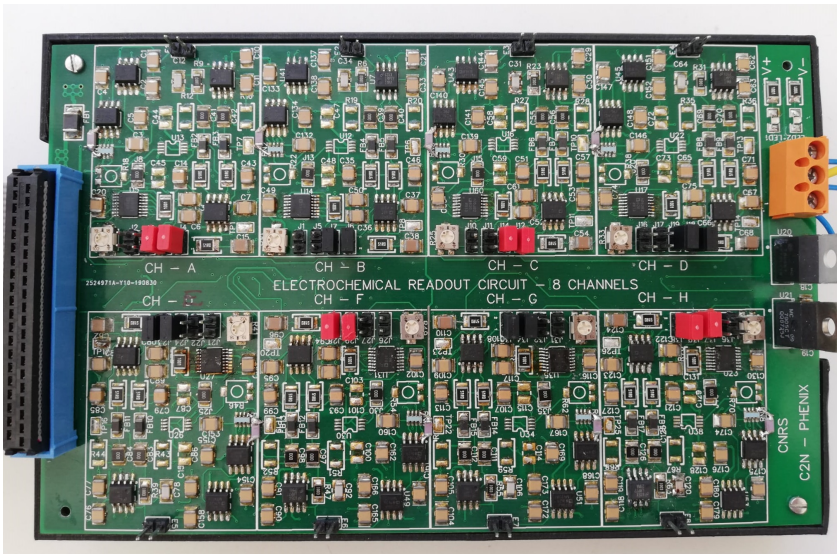

Figure 3.16: Electronic board to perform the electrochemistry detection, 8 measurements at the same time can be performed.

3.3.1 Simulations for the WE part

In this section I will report the simulation done under the electronic setup already explained for what concerns the WE part, so regarding the current measurements.

It has to be kept in mind that the aim of this step is to read the current values, this is only possible by amplifying it and converting into a voltage to make it readable by the ADC that will transmit the values to the microcontroller and so to the LabVIEW interface.

The Cyclic Voltammetry measurement consists in measuring the current signal obtained form the WE when a triangular shaped voltage is applied to the electrodes (2.3.3). This current signal ranges between 1 to $500nA$, and it is collected at the WE, the aim is to measure it during the applied voltage signal.

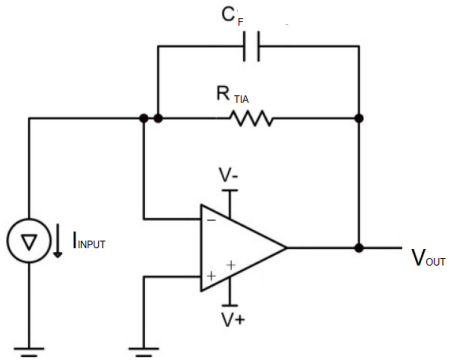

Figure 3.17: Schematic of a TIA circuit.

In the first step the current signal is amplified and converted into a voltage signal, this is accomplished thanks to a transimpedance amplifier (TIA), the circuit is depicted in Figure 3.17. General TIA circuits have only a resistor (R_{TIA}) in the inverting part. The output voltage of a TIA is equal to $V_{OUT} = -I_{IN}R_{TIA}$, in fact the gain is entirely related to the resistor and always negative due to the fact the output is given as feedback to the inverted terminal.

However, in order to increase the stability, a feedback capacitor (C_F) is introduced in parallel to the TIA resistor [71, 72]. Moreover, the introduction of the capacitor introduces a pole in the Bode diagram, such that it works as a low pass filter.
The transfer function of the circuit will be as follows:

$$H(j\omega) = -\frac{R_{TIA}}{1 + j\omega C_F R_{TIA}} \tag{3.9}$$

so the pole frequency is $f = \frac{1}{2\pi C_F R_{TIA}}$. This means that by increasing the capacitance the bandwidth will be shorter.

Anyway, the value of this feedback capacitance must be chosen accurately for providing a good stability and compensation. In fact, these types of circuits can present hidden parasitics that cause instability problems [73].

Feedback capacitor analysis

In this first step, the TIA circuit is simulated, by considering the input current (I_{IN}) represented in blue in Figure 3.19, so an hypothetical the square wave input current between $\pm 50nA$ with a period of 10ms.
At first the two supply voltages V_{CC} are set to $\pm 5V$, the resistor R_{TIA} is set to $100k\Omega$ for providing good amplification and ensuring a large bandwidth.The capacitor C_F is changed during the simulation and set to 10pF, 100pF and 1nF.

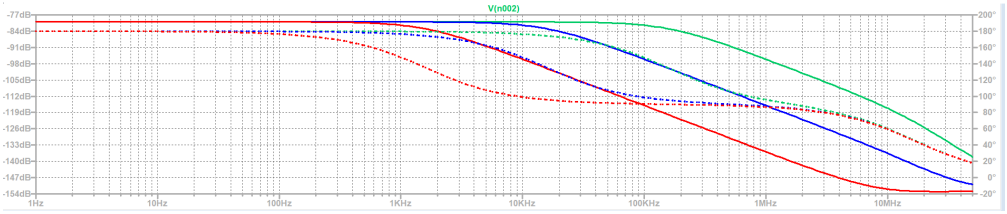

Figure 3.18: Bode diagram for R_{TIA}= $100k\Omega$, C_F = 10pF (green line), 100pF (blue line), 1000pF (red line).

In Figure 3.18, it is possible to observe the obtained Bode diagram, the dashed lines represent the phase of the frequency response and the continuum lines represent the amplitude. The maximum gain for the three cases is $G = -80dB$, this is obvious due to the fact that the resistor is kept constant. The green line is for the case C = 10pF, the blue line is for C = 100pF, red is for C = 1nF.
In the following table (3.1) the cut off frequencies in the three cases are reported:

C_F	f_P	G
$10pF$	$160kHz$	$-80dB$
$100pF$	$16kHz$	$-80dB$
$1nF$	$1.6kHz$	$-80dB$

Table 3.1: Simulation by changing the feedback capacitor, $R = 100k\Omega$

The pole frequency should be low enough to cut lot of noise, such that the final current signal can be significantly clear. By the moment, we can say that a reasonable cut off for the filter could be on the order of $10kHz$, in fact by considering an input signal with a period of 10s, on which we want to take 10000 measurements, we will work at a frequency of around $1kHz$, so to be sure we can

consider $10kHz$ as our cut off frequency.
For that reason, by evaluating the pole frequency, it is possible to say that a feedback capacitor of the order of $100pF$ could assure the good bandwidth, anyway this is not enough to point this feedback capacitor as the best. In fact we should also check that this capacitor value assures both a **good linearity in the response**.

The good linearity can be checked in the transient response. In Figure 3.19 it is possible to observe the transient response for the three different feedback capacitor already mentioned. The blue line is the input current, while the green one is the output voltage. At first it is possible to notice that the latter one is between $\pm 5mV$, in accordance with a gain of 100k. It is also observable that the response delay is on the range of $\approx 0.8ms$. Moreover, there are no visible changes in the transient response by changing the capacitor in this range of values, so it is possible to say that these values guarantee a good response.

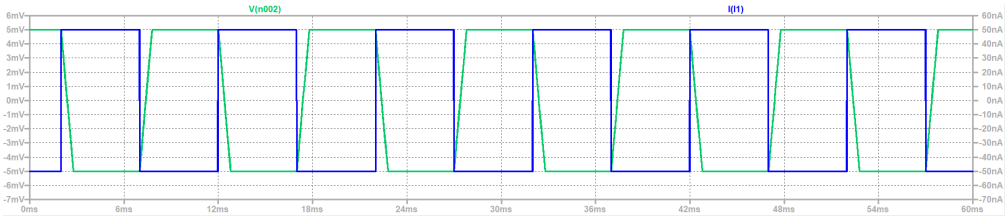

Figure 3.19: Transient response for R_{TIA}= $100k\Omega$, C_F = 10pF, 100pF, 1000pF . The blue line is the input current signal, the green line is the output voltage.

However, when the capacitor value is too high, for instance $C_F = 5nF$ the output voltage cannot follow anymore coherently the input current, as it is possible to see from figure 3.20. For that reason it is possible to fix C = 1nF the maximum capacitor value to assure a good transient response.

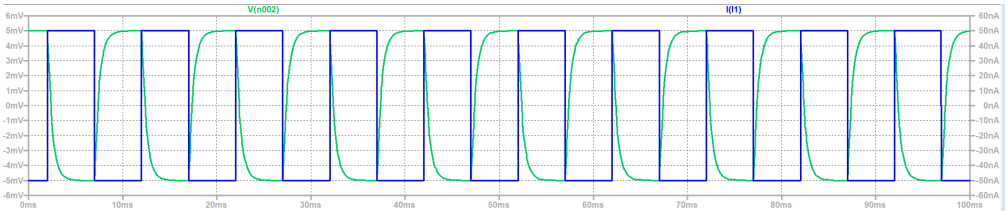

Figure 3.20: Transient response with C_F = 5nF.

Finally, it is possible to say that the analysis to find a correct value of capacitor for a TIA circuit by fixing a resistor should be taken into account:

- the study of the frequency pole to assure a bandwidth large enough;
- the study of the maximum value to guarantee a good transient response.

TIA Resistor analysis

Afterwards, the resistor R_{TIA} is studied by fixing the capacitor to 100pF, in order to study both the bandwidth and the gain. $R_{TIA} = 10k\Omega$, $100k\Omega$, $1M\Omega$ are the analyzed values and the Bode diagram is depicted in Figure 3.21. As expected both the gain and the f_P change as reported in table 3.2.

R_{TIA}	f_P	G
$10k\Omega$	$160kHz$	$-100dB$
$100k\Omega$	$16kHz$	$-80dB$
$1M\Omega$	$1.6kHz$	$-60dB$

Table 3.2: Simulation by changing the resistor R, C = 100pF.

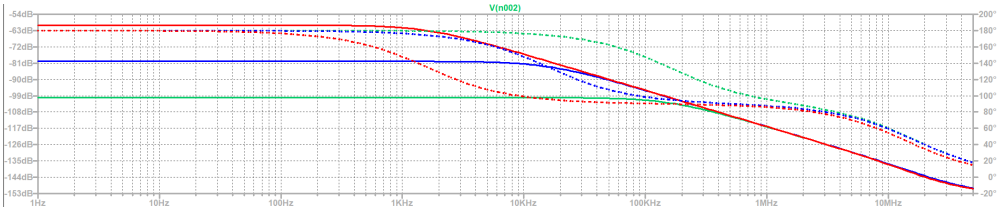

Figure 3.21: Bode diagram with $C_F = 100$pF, $R_{TIA} = 10k\Omega$ (green line), $100k\Omega$ (blue line), $1M\Omega$ (red line).

Again, it is possible to observe that even if the resistor $R_{TIA} = 10k\Omega$ guarantees a larger bandwidth, a gain of 10k could not be enough to amplify the signal, and the opposite happens with $R_{TIA} = 1M\Omega$. For that reason, a value of $R_{TIA} = 100k\Omega$ could be a good compromise for both the bandwidth and the gain.

Instrumentation amplifier Gain

The next study is finalized to guarantee a correct input for the ADC converter, it will be treated by keeping $R_{TIA} = 100k\Omega$ and $C_F = 100$pF. The ADC converter to use is a LTC2309 converter, from its datasheet it is possible to see that it requires an analog input of : $\pm 2.048V$.
As seen in Figure 3.19, by choosing a TIA resistor of $100k\Omega$, the voltage at the output of the TIA circuit on the order of $\pm 5mV$. For this reason, the signal has to be further amplified to be converted into a digital signal, this is possible by using an instrumentation amplifier, in such way it is possible to adapt the the signal to the dynamic range of the converter.
The operation amplifier chosen is a AD8220, from its datasheet it is possible to

read that the gain is defined by the following formula:

$$G_{IA} = 1 + \frac{49.4k\Omega}{R_G} \tag{3.10}$$

This means that if we want an adequate input for the ADC converter, we can consider that the minimum square amplitude input voltage can be of 1 V and the maximum can be of 4 V. For that reason, a reasonable gain can be from 100 to 400. By replacing this value in the previous equation it is possible to find a minimum resistor $R_G = 125\Omega$ for obtaining an output voltage oscillating between $\approx \pm 2V$ (amplitude = 4V), and a maximum resistor value of $R_G = 490\Omega$ for having an output voltage oscillating between $\approx \pm 0.5V$ (amplitude = 1V).

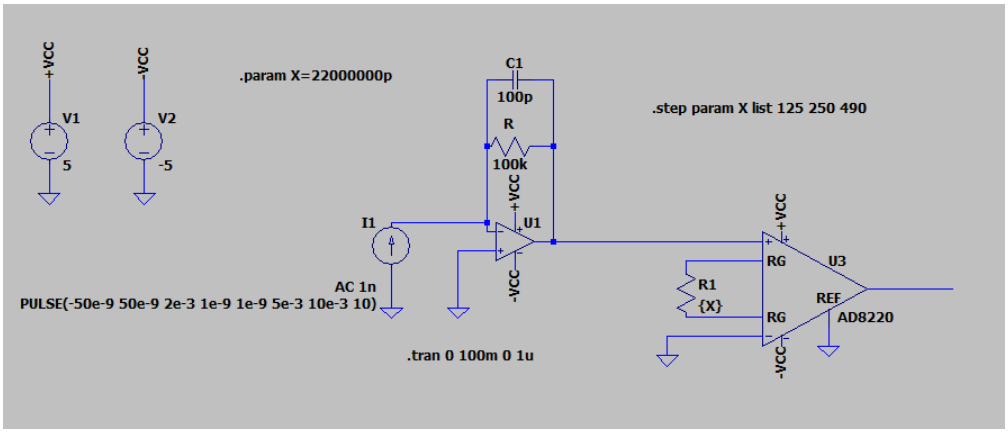

Figure 3.22: Schematic of the circuit: TIA plus instrumental amplifier.

In Figure 3.22 it is possible to observe the schematics already explained: the input signal I1 pass through the TIA circuit, and then is further amplified thanks to an instrumentation amplifier (AD8220), in order to guarantee a correct signal (range of $\approx \pm 2.048V$) for the analog to digital converter (LTC2309).
Figure 3.23 shows the output voltage at the end of the instrumentation amplifier, by using the following resistors $R_G = 125\Omega$ (red line),250Ω(light blue line), 490Ω (pink line). For $R_G = 125\Omega$ the gain is 396, so the output voltage is $\approx \pm 2V$, for $R_G = 250\Omega$ the output voltage is $\approx \pm 1V$ and for $R_G = 490\Omega$ the output voltage is $\approx \pm 0.5V$.

Potentiometer

Even if the previous simulations are realized by considering the resistor R_G fixed, now the idea is to put a variable resistor, a digital potentiometer, instead of a fixed one.
In this way, the gain of the instrumentation amplifier and so the gain of the circuit

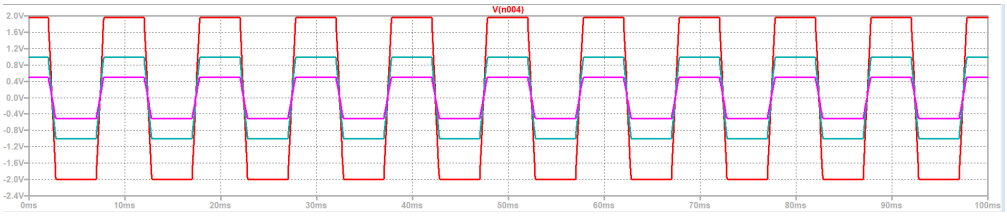

Figure 3.23: Output voltage after amplification due to instrumental amplification. $R_G = 125\Omega$ (red line),250Ω(light blue line), 490Ω (pink line).

can be adjusted and monitored by the user thanks to the LabVIEW interface. The used potentiometer is an AD5262, from its datasheet it is possible to read that the resistor value varies from 60 Ω to 20 $k\Omega$. However, in order to obtain an higher gain, we are interested in the smaller range of R values, for that reason two resistors are put in parallel. This is also useful to have a more accurate value, in fact when two resistors are put in parallel the tolerance is reduced.

The digital potentiometer adjust the resistor depending on a *Code Gain* set by the user. In order to have precise information about the relation between the set Code Gain and the value of the resistor, and so the gain of the circuit, the resistor values are measured thanks to the use of a multimeter tester by changing the code gain. In Figure 3.24 it is possible to see the obtained values for one channel of the board, an interpolation fit is also done in order to verify the linearity of the curve, and it is plotted on the same image. The obtained equation from the fit is the following one:

$$R_G = m * CG + q \tag{3.11}$$

where CG is the Code Gain, and m and q are the slope and offset respectively, they vary for each channel, in the table 3.3 are reported these fitted value for each channel of the board.

	m	q
CH A	-39.81	10251.81
CH B	-40.27	10369.84
CH C	-39.49	10170.35
CH D	-40.70	10485.50
CH E	-39.44	10158.05
CH F	-40.22	10356.25
CH G	-40.81	10507.46
CH H	-40.98	10553.36

Table 3.3: m and q fitted parameter from equation 3.11

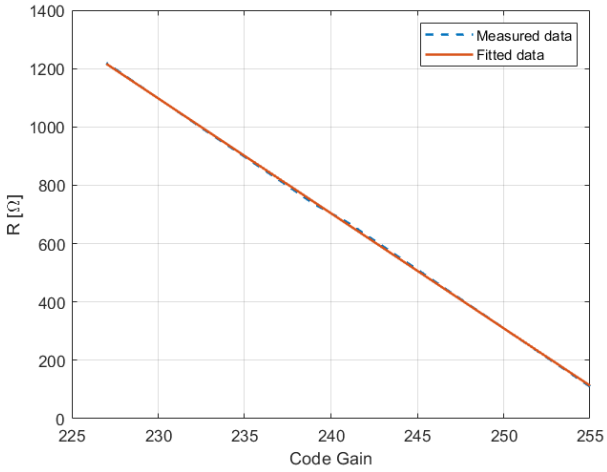

Figure 3.24: The red curve represents the measured resistor respect to the code gain sent, the dotted cure represents the linear fit.

After that, the resistor values are replaced in the equation 3.10 of the Instrumentation Amplifier Gain , in order to give a correspondence between the resistor values and the IA Gain, this is plot in Figure 3.25a. By using the data obtained from the fit the resulting gain will be as follows:

$$G_{IA} = 1 + \frac{49.4k\Omega}{m * CG + q} \tag{3.12}$$

where CG represents the Code Gain and m and q depend on the channel.

Moreover, in Figure 3.25b the IA gain is plotted respect to the potentiometer code gain.

As seen in the previous section, the range of the IA gain, by considering a current of $\pm 50nA$, is between 100 and 400, which corresponds to a value of resistor between 490Ω and 125Ω. By replacing this value in Figure 3.25b, in order to check the values of the Potentiometer Code Gain, a reasonable range is between 245 and 254. These values are interesting because they are the parameter to send to the microcontroller from the LabVIEW interface.

However, the simulation is performed by considering a value of current of $\pm 50nA$, but the obtained current from the working electrode could be even higher. This fact really affects the measurement and the simulation done. Indeed , if the set gain is too high and the received current is of the order of hundreds nA, the output signal will be cut, because the input signal for the converter will be too high respect to the one supported by the ADC and we would have a saturation in the measured current.

Therefore, it is possible to establish a minimum gain for the controller, for the

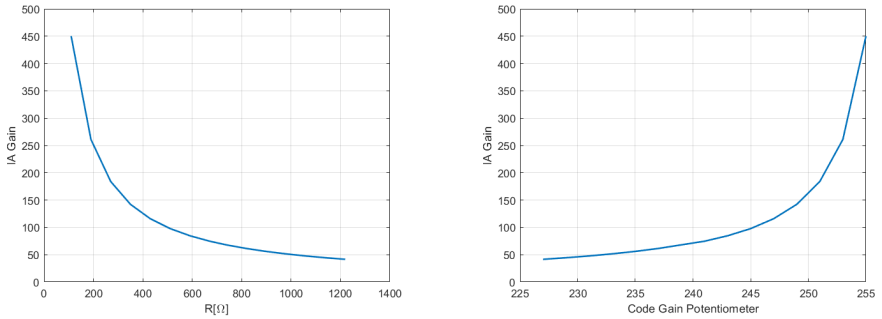

(a) IA Gain respect to the resistor value of the potentiometer.

(b) IA gain respect to the Potentiometer Gain Code.

Figure 3.25: Gain simulation done by following the measured value of the resistor in Figure 3.24.

case of maximum input current from the WE. In fact, by considering a maximum current of 500 nA, in order to have an input voltage for the ADC of 2V, we need an IA gain of 40, which corresponds to Potentiometer Code Gain of 227.
Moreover, it is also possible to establish a maximum gain for the controller. In this case, for a minimum input current from the WE, it is possible to say that the maximum Potentiometer Code Gain is 255 (from the potentiometer datasheet), in such way an IA gain of 450 is guaranteed.
It is finally possible to say that the range Code Gain at which we are interested is between 227 and 255.

Low pass filter (Anti-aliasing filter)

Even if a low pass filter is provided by the transimpedance amplifier, the obtained signal is still noisy. This is possible to see from Figure 3.26a, for that reason, a further low pass filter is introduced after the instrumental amplifier.
In particular a resistor of 51Ω and a capacitor of 1.5μF are set at the output of the instrumental amplifier. As it is possible to see from Figure 3.26b, by the introduction of the low pass filters, the noise is significantly reduced.

Finally, in Figure 3.27 is plot the transfer function of the circuit after the introduction of the filter. It is possible to notice that the cut off frequency is at $\approx 2kH$.

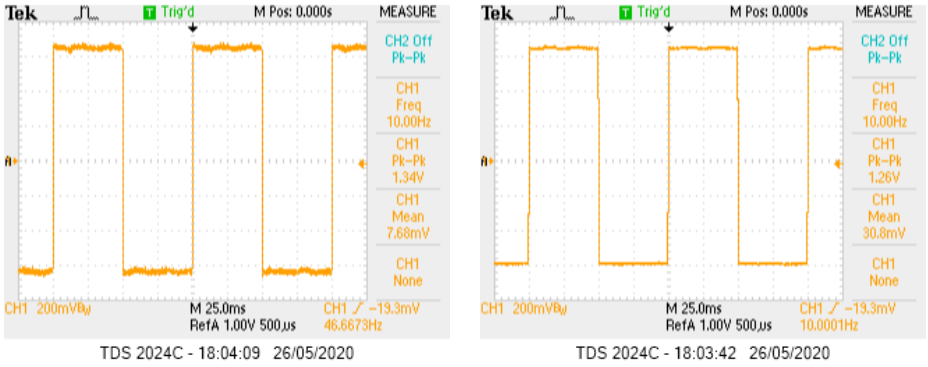

(a) Output current after the IA, without the use of a further low pass filter.

(b) Output current after the IA, with the introduction of a low pass filter.

Figure 3.26: Differences of the output signal by introducing a low pass filter, it is possible to notice that in the second case the signal is less noisy, measurement done with the oscilloscope.

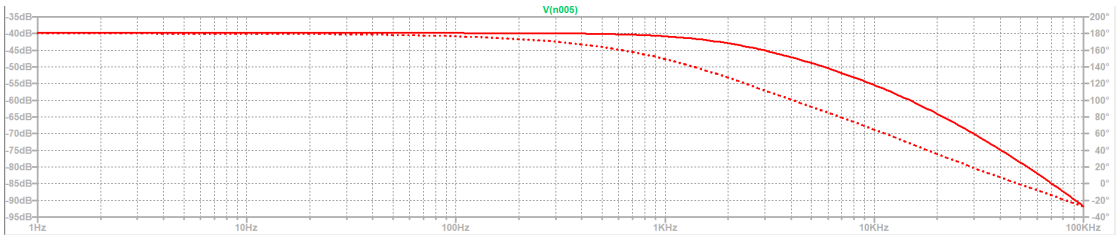

Figure 3.27: Transfer function from a *LTspice* simulation with the introduction of the low pass filter.

3.3.2 Experimental analysis for the WE part

Now that the simulations are done, it is necessary to experimentally prove the validity of the circuit.

At first, it has to be checked that the current measured at the WE corresponds to the real value of current received, for each code gain sent for the potentiometer.

Then the frequency analysis is done after each filter, for different values of gain.

Gain analysis

In order to perform the gain analysis, a voltage generator is used to send a sinusoidal signal of $1V$ peak-peak , this is connected in series with a resistor, $R = 10M\Omega$ (measured value = $9.978M\Omega$), and so a sinusoidal current with an amplitude of 100nA is sent at the WE ($I_{input} = V_{input}/R$).

Now, thanks to the use of an oscilloscope, the output voltage is measured at the output the Instrumentation Amplifier, after the low pass filter. These values of voltages are measured by changing the gain between 227 and 255, for each of the 8 channels of the board.
The data are converted into gain in mV/nA and plotted with MatLab for each channel ($Gain[mV/nA] = V_{measured}[mV]/I_{input}[nA]$) respect to the Code Gain inserted.
This gain that we are calculating is the Gain of the black box that contains two stages of amplification (TIA + IA) and the filter, according to Figure 3.28.

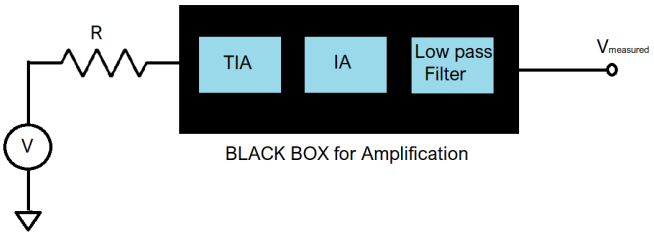

Figure 3.28: Black box on which the total gain is measured.

The total measured gain, by neglecting the low pass filter transfer function that at the working frequencies is supposed to be equal to 1, has to have a behaviour as follows:

$$G_{total} = G_{TIA} * G_{IA} \tag{3.13}$$

from which we know that the G_{TIA} is $100kV/A$ ($0.1mV/nA$), and the G_{IA} according to the equation 3.12.
In Figure 3.29, it is possible to see the differences from the theoretical gain (blue) and the experimental gain (red) for the first channel (CH A).

Now a fit of the obtained measured black box gain is done for each channel. The fit is done by using the function `lsqcurvefit` with Matlab on which the parameters A and B from the following equation are extracted:

$$G_{total} = A\left(1 + \frac{B}{m * CodeGain + q}\right) \tag{3.14}$$

In the following table (3.4) all the A and B values are reported for each channel, by taking into consideration the m and q values calculated before for each channel.

Finally, in Figure 3.30 all the experimental gains and the respectively fit are plotted for each channel.

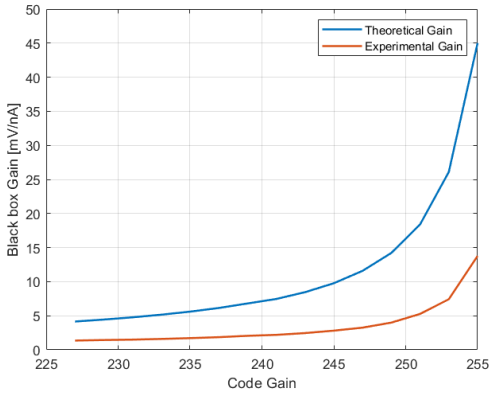

Figure 3.29: Comparison between the theoretical black box gain and the measured one.

	A	B
CH A	0.14	9480.43
CH B	0.29	4507.09
CH C	0.62	1996.33
CH D	0.17	7929.26
CH E	0.54	2463.03
CH F	0.18	7273.04
CH G	0.17	7889.49
CH H	0.21	6496.50

Table 3.4: A and B fitted values from equation 3.14

Frequency analysis

Then, the frequency analysis is performed in order to check the validity of the filters, this is done only for one channel. This is done in 3 point of the circuit, due to the fact that the total circuit has 3 filters:

1. The first filter is the Transimpedance Amplifier (TIA, Figure 3.15), the cutoff frequency should be of $f = 16kHz$.

2. The second filter is not mentioned in Figure 3.15, it is between the TIA and the IA, so the measurements are taken immediately after the Instrumentation Amplifier.

3. The last filter is the low pass filter after the IA, figure 3.15.

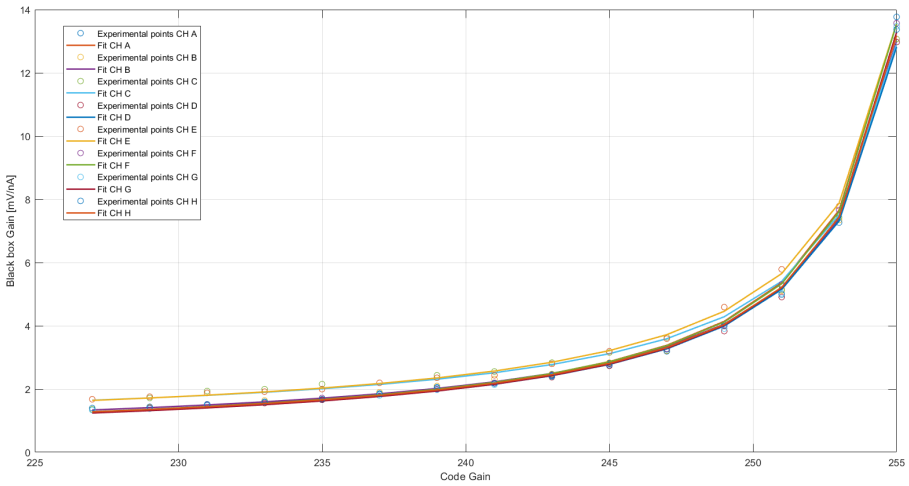

Figure 3.30: Experimental gain values with the respectively fit for each channel.

In order to perform these measurements, again a voltage generator is used. A sinusoidal signal is sent with an amplitude of 1 V and a resistor of $10M\Omega$ is put in series in order to generate an input current oscillating around $100nA$ (as showed in Figure 3.28). The obtained output voltages are measured at each of the three points mentioned above, and the frequency is swept by the use of the generator.

For the first point, the TIA filter is analyzed. The voltage amplitude values are converted into Gain in $[mV/nA]$, in fact it is divided by the value A (for the corresponding channel) in the equation 3.14 that represents the fitted value of the TIA gain. These gain values are plotted respect to the frequency as showed in Figure 3.31.

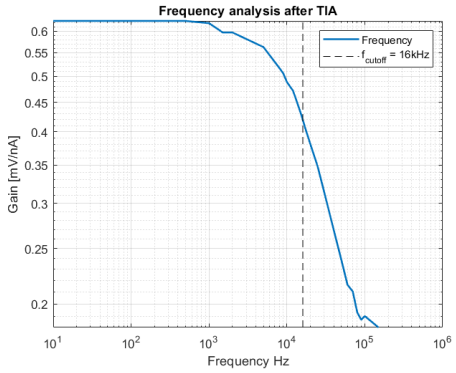

Figure 3.31: Experimental frequency analysis after the TIA stage.

The theoretical cut off frequency is one equal to $16kHz$ (dashed black line), as proved from the previous simulations. While the experimental one (the frequency at which Gain = $maxGain/\sqrt{2}$) is around 14kHz, so a little lower respect to the theoretical one.

For what concerns point 2, the measurement is performed in the same way. The only difference is that now the analysis is also done by checking different values of gain. Due to the fact that the bandwidth product has to remain constant, by lowering the gain, we should see that the cut off frequency will be higher and vice versa. The analyzed code gains are three : 255 (maximum), 241 (medium), 227 (minimum). Again, the collected output voltage is converted into Gain from the equation 3.14, but in this case the G_{total} is considered, due to the influence of both the TIA and IA gains.

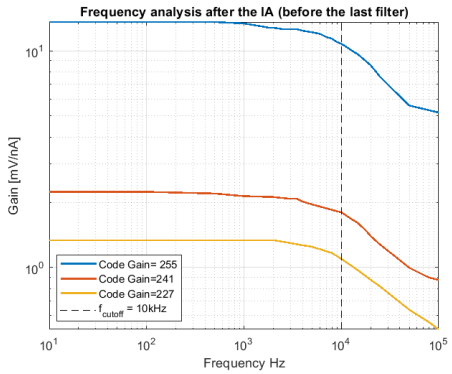

Figure 3.32: Experimental frequency analysis after the IA stage.

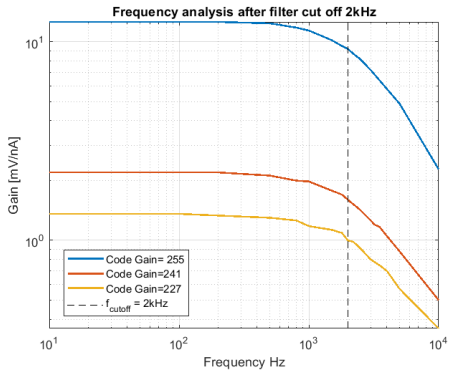

Figure 3.33: Experimental frequency analysis after the low pass filter stage.

In the circuit a capacitor of 330pF is put in parallel with a resistor of 51Ω, so the theoretical cut off frequency is $\approx 10kHz$.

In Figure 3.32the results are plotted . It is possible to observe that in this case the theoretical cutoff frequency corresponds quite well with the experimental one. Moreover, as expected, by enlarging the gain, the cut off frequency is lower (due to the fact that the gain band-width product must remain constant).

Finally, in the same way, is analyze the point 3: after the low pass filter, the results are plotted in Figure 3.33. Again, it is possible to observe that the gain-bandwidth product is constant and that the theoretical cut off frequency of 2kHz is quite respected in the experimental analysis.

3.3.3 Software part treated

Now that all the hardware part is treated, I will explain a function that I implemented in the microcontroller code, to adjust the gain in an automated way.
After that I will explain an external Matlab code that I wrote, to treat and analyze the data.

Autorange gain

This function is created in order to perform measurements with an automated gain control, this is necessary in order to avoid saturation current problems and noise problems. In fact, as said, it is possible to choose the code gain to set from the LabVIEW interface in the setting parameters. However, choosing the gain parameter is difficult in particular if the user doesn't know in which range will be the obtained current.
Moreover, if the set gain is too high, it is possible to encounter some saturation problems. In this case, the current will be converted and amplify to a voltage value too high to be correctly converted from the ADC.
On the other hand, if the set gain is too low, the obtained current will be highly noisy.
For these reasons, a function for having an autocalibration gain is implemented.

In order to do it, at first, the experimental ADC input values that will provide the saturation of the signal are checked. In fact, despite the theoretical ADC input voltage values are ± 2.048 V from the datasheet, it is possible to check that it start saturating in the ± 0.5 V range.
So, the microcontroller code is changed such that, the parameter set by the user will correspond to the maximum gain. The program will start performing the measurement and if it will start saturating so entering in the condition of which the input voltage for the ADC is larger than 500 mV or lower than -500 mV, the code gain will be automatically lowered of 1 unit. In such way after few measurements it finds the optimum gain avoiding both saturation and noise. In fact this optimum gain will be the maximum gain before the saturation, and so enough high to avoid

the noise. This method will provide a clear signal in a faster and automated way.

In Figure 3.34 it is possible to see an example of measured current respect to the time, it is possible to see that in the first cycle the current is cut due to the fact that it saturates, in fact the initial code gain was set to the maximum: 255. However, already from the second cycle it is possible to see a really clear signal, this is because in the first cycle the code will arrange the gain, and from the second cycle the gain is the optimized one for each point.

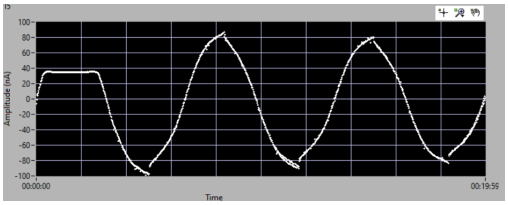

Figure 3.34: Current respect to the time during a measurement.

Data analysis

The aim now is to analyze the data acquired in this process, in fact when the user perform a measurement will have lot of data to analyze. In order to manege all the data in a simple way, I wrote a $MATLAB$ő code to open the data file, read and analyze them. In this subsection I will explain briefly what the program does.

The obtained data from the electronics instrumentation will contain the voltage and the current measured for each cycle performed. In fact the electronic instrumentation sends a signal from 0 to the maximum voltage V1, then from V1 goes to V2 and from V2 to 0 for each cycle, as explained in Figure 3.3a. So the aim at the beginning is to open the files and read and saved the IV matrix, having in the raw the values acquired for each column that represents the number of cycle.

Now, in order to analyze the data they are ordered in two main parts: the ascending signal, so the one from the maximum V_1 to the minimum V_2 (by keeping in mind Figure 3.3a); and the descending signal, from V_2 to V_1.

In this way, for each cycle we will have these two signals to analyze, this is important because the two signal, especially in static analysis do not always correspond perfectly.
Then, for each part, the figure of interest will be mainly three, from Figure 3.35:

- the maximum peak, in general a plateau if we are in static, or with a low scan rate;

- the slope of the middle part;

- the minimum peak, in general a plateau if we are in static, or with a low scan rate.

For this reason, it is important to find a general way to split the graph in these three main part in order to do three linear fit. This is done by first individuating the plateaus.

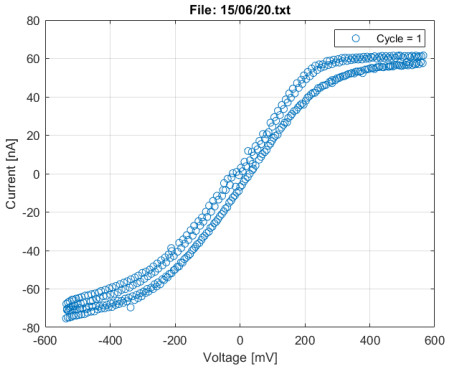

Figure 3.35: Example of a general signal obtained from the CV measurement.

The individuation of the plateau is done by creating a threshold value. In fact, at the beginning of the program, two variables called `num pl max` and `num pl min` are stored, these numbers represents the numbers of maximum (and minimum) used to individuate the average plateau. In fact an average of these `num pl max` and `num pl min` (in general 40 points are set), is performed and stored as `plateau max` and `plateau min` respectively. Then a delta is calculated as the distance between the absolute maximum (minimum) and the `plateau max` (`plateau min`). Finally this delta is subtracted (added) to the value of the `plateau max` (`plateau min`), and the value obtained will be the threshold value.

Now, that we have the minimum and the maximum threshold, it is possible to split the graph in the three different parts in order to do the linear interpolation. The result is plotted in Figure 3.36.

3.3.4 Perform the full protocol

Now that both the magnetic hyperthermia and electrochemical protocol are treated. A final step is needed: to create a function where it is possible to unify the two protocols. In this way the user have just to insert the setting parameters, and leave the electronics instrumentation to perform the whole protocol.

This $perform\ full\ protocol$ stage is added as a new state to the microcontroller code explained in image 3.2 at the beginning of the chapter, so a total new stage implemented to increase the functions that the instrumentation can perform.

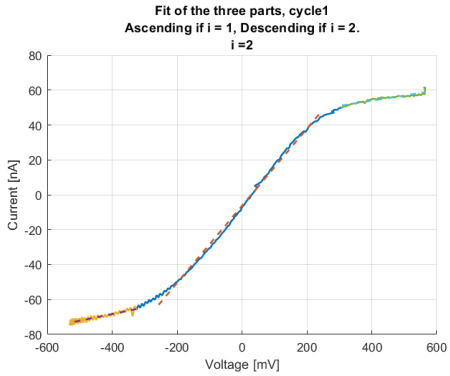

Figure 3.36: Example of the fitted signal obtained from the CV measurement, only descending part from image 3.35 represented.

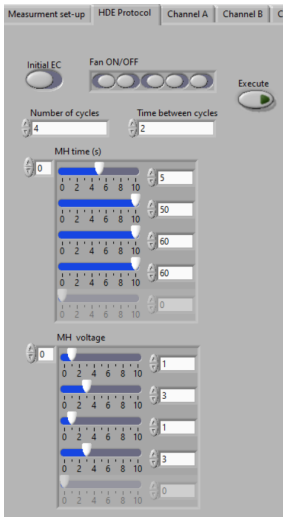

Figure 3.37: Full protocol interface. Addition parameters to insert for preforming the full protocol.

The parameters to insert are the following ones:

- the parameter entered in the electrochemistry protocol;
- the frequency and span in the magnetic hyperthermia protocol;
- the number of cycles to perform (one cycle contains the magnetic hyperthermia protocol + electrochemistry protocol);
- the time between each cycle in seconds;
- if before doing the first cycle the user wants to perform an EC measure;

- if the user wants the fan to be on or of for each cycle;
- the duration of the magnetic hyperthermia protocol for each cycle;
- the voltage supplied to the H-bridge for the magnetic hyperthermia protocol for each cycle.

The interface for this is displayed on Figure 3.37.

3.4 Chapter conclusions

In this chapter I explained the electronics instrumentation that makes working the microfluidic device in an automated way and what I did to improve the performances of it.

In particular, for what concerns the magnetic hyperthermia protocol, my work was mainly based on coding in C++ the microcontroller to realize the protocol. The function to find the resonance frequency was implemented, this useful tool let the system working at the lower impedance conditions, so the highest current and magnetic field can be provided. Then the function to perform the magnetic protocol at the time and the voltage insert by the user and the resonance frequency found was also performed.

For what concerns the electrochemistry part, I worked in *LTSpice* simulations in order to justify the choices of the elements for the working electrode part. Then, I did the characterization of some elements, such as the experimental gain for the transimpendance amplifier plus the instrumentation amplifier. These characterizations and the successive fits are done for each channel of the device, such that, by inserting the final function of the total gain found in the code of the microcontroller, it is possible to plot on the *LabView* interface real values of obtained current.
Then, the characterization in frequency of every filter present in the WE circuit is done, thanks to them it is possible to reduce a lot of signal noise and to have a final filter cut off of 2 kHz.
Also in the electrochemistry part I implemented a function for the microcontroller code, this function is for the gain auto-adjusting in the instrumentation amplifier, thanks to the use of the digital potentiometer. In such way, the gain is optimized for every measurement, in fact the dynamic range of the amplification is adjusted to the dynamic range of the ADC in an automated way.
Finally, I realized a *MATLAB* code for the data analysis, such that it is possible to directly insert the file generated by the LabView interface in the folder, and it will be possible to have the fit for the three parts of the curve: the mean value of the negative plateau, the slope of the central part, and the mean value of the positive plateau.

In the end, the last thing implemented is a new state in the microcontroller code, for the realization of the full protocol. There, the new parameters for realizing a full protocol of maximum five cycles where every cycle contains the magnetic hyperthermia protocol plus the electrochemistry measurement.

Chapter 4

Fabrication process of the device and experiments

Now that all the electronics instrumentation is explained, the interest goes to the realization of the experiments. In fact, in this last chapter I will explain the fabrication process for the realization of the LOC and the experiments held regarding the EC part to characterize the microfluidic biosensor.

Even if I did not assisted to all the fabrication parts of the device, it is interesting to report the physical processes exploited for the realization of the device, in order to highlight the simplicity of it. In fact, the easiness and cheapness are some of the purposes of this device.

Unfortunately, I did not have the opportunity to test the magnetic hypertermia protocol with the magnetic nanoparticles, because the nanoparticles fabrication was temporarily suspended. However, with this last work of experiments I had the opportunity to prove the validity of the electrochemical board and protocol.

In particular, in the experiments reported, I worked on all the steps of the electrochemistry protocol: the characterization of the bare electrodes, the functionalization of the electrodes and the hybridization with complementary targets in different concentrations.

With these results it is possible to show the validity of the electrochemistry instrumentation. Moreover, in the first part I report an experiment done on which eight measurements are taken at the same time. The results show a really clear signal as a prove that the EC board can afford more measurements at the same time, so the multiplexing capability is confirmed.

4.1 Fabrication process

As already explained, the physical process for the realization of a LOC should be really easy and should permit the parallelization in order to decrease the costs of the own device.

The main materials of the device are: a glass substrate where it is deposed the pattern for the electrode and the PDMS layer used to cover the glass to form the channels. The electrodes material can be usually gold, platinum or amorphous carbon nitride (a-CNx).
Despite the fact that the Au provides a small potential window (the applied voltage used is not larger than $\pm 0.2V$) , it is the most used because on it the functionalization is easier and it reduces the cost and time of the fabrication. The Platinum, for istance, is used sometimes for the CE, but never for the WE, because on it the functionalization is impossible. The a-CNx is more stable than gold, and it provides a larger potential window, but it has to be activated with KOH or H_2SO_4 before functionalization, that's why this process is longer and so more subject to errors.

In the following I will report the steps for the fabrication process.

- Electrodes fabrication.
- Microchannel mold fabrication.
- Plasma bonding.

Electrodes fabrication

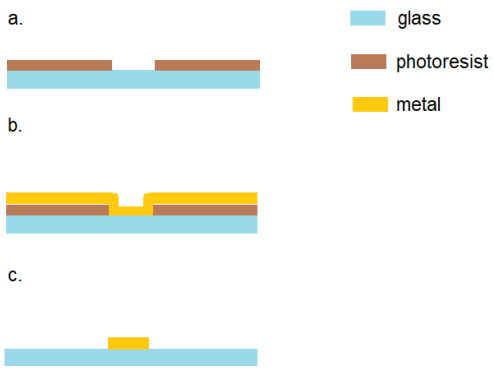

Figure 4.1: Schematics of the physical process for electrodes realization on a glass substrate.

The electrodes are patterned on a glass substrate thanks to the use of a soluble resist by a lithographic process. In fact, as depicted in Figure 4.1 at first the resist patterns the negative of image we want to obtain (a), by the use of a mask. Then, the electrodes material is deposited by sputtering (b). And finally, by the lift-off, the resist is removed (c) using the acetone as solvent able to completely remove the resist, the final result is the glass plus the electrode.

The working electrode (WE) is 30μm by 300μm and the counter electrode is 2 mm by 300μm.

Microchannel mold fabrication

The PDMS is realized such that it contains all the channels pattern, the process is depicted in Figure 4.2. At first a SU-8 master mold is realized on a Silicon wafer, thanks to the lithography (a. before lithography and b. after). Then, a layer of PDMS is poured on the SU-8 master mold that contains the channel pattern (c) [37]. Finally, it is insert in the oven at 70^{o}C for at least 4 hours. Now it is possible to peel off the PDMS from the substrate (d). The PDMS in this way will have the pattern of the channels.

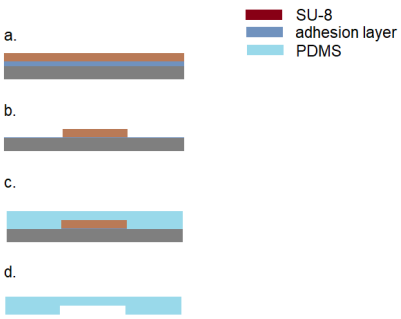

Figure 4.2: Schematics of the physical process for the PDMS realization.

Plasma bonding

Now the glass with the electrodes and the PDMS are cleaned with isopropanol and dried [37]. The holes for the intlets and outlets are manually created by a special cutter. Finally the two parts can bond together thanks to the nitrogen plasma that guarantees a good adhesion of the substrate with the PDMS. The manual alignment is realized.

4.2 Measurements

In this section I am reporting the electrochemistry experiments done by the use of the electronic instrumentation, in order to prove the validity of the electrochemistry board. In particular, several experiments are realized with two main different types of devices, and the main results will be explained in this chapter.

The protocol for the realization of the miRNA quantification, by the use of the CV measurements, consists in the following three main steps:

- the CV measurement is performed with bare electrodes, only the electrolyte (ferri/ferrocyanide 3 mM) is insert in the microfluidic device.
- the electrodes are functionalized with the capture probes (synthetic probes complementary to the targets we want to analyze). The CV measurement is realized.
- the reporter probes are inserted (miRNA targets under detection). The CV measurement is again performed.

Even if the last measurement is the one that permits the probes quantification, we are not interested in the absolute value of current, because, depending on the electrodes, it can varies from one pair to another. In fact, some electrodes can present different characteristics on the surface that really influences the current values depending on their geometry, material, fabrication process, conservation, that is why we need to compare the last measurement with the previous two. The relative measurements are interesting also to check that the protocol worked, in fact, it has still to be perfectioned due to the fact that sometimes the hybridization does not occur.

Anyway, from this measurements, it will possible to appreciate that after the functionalization, the current will decrease, due to the fact that the microRNA capture probes will cover the electrodes and so the faradaic processes are reduced, the result is a lower current. It will be possible also to observe a changing in the shape of the CV curve due to the decreasing of redox reactions. When the reporter probes will be introduced the hybridization will take place between complementary targets. In this way, the surface electrodes will be more covered by the double strand probes and, as a consequence, it will be possible to appreciate again a reduction of the current in the CV measurement. It is also observable that, by increasing of the reporter probes concentration, the current will decrease, due to the fact that the surface electrodes will be more covered.

In this case, the reduction of the current is always possible due to the fact that no Methylene Blue is inserted in the electrolyte. In fact, on the other hand, by adding an intercalant in the electrolyte, the current will increase directly proportional to the covering of the electrodes surface.

Material of the electrodes	Au/Au
Electrolyte	Fe_{II}/Fe_{III}
Type of miRNA under detection	miRNA 122
Pump flow rate	0.5 $\mu L/s$
Initial voltage V_i	0 V
Intermediate voltage V_1	0.2 V
Intermediate voltage V_2	- 0.2 V
Final voltage V_f	0 V
Voltage scan rate	0.05 V/s
Number of samples	400
Number of cycles	2
Number of samples per point	2
Maximum code gain	255
Integration time	0.01 %

Table 4.1: Conditions of the experiments.

In table 4.1 are reported all the conditions used for the experiments, in particular, in the first four lines are reported the general conditions of the experiment, and then the electronics parameters already treated at the beginning of chapter 3.

The devices used have Au/Au electrodes (WE/CE), even if other materials are subject of study in the team. However, the gold has not a large potential window, that is why the peak to peak voltage provided is always 0.4 V and the scan rate provided is 0.05 V/s in order not to damage the electrodes. As already mentioned, the electrolyte used is the Ferri/Ferrocyanide, without the use of intercalant.
The type of miRNA under detection is the miRNA 122, the complementary capture probes exploited are thiol-labeled DNA, such that the thiol can easily attach to the gold electrode to form a self-assembled-monolayer (SAM), in Table 4.2 the sequence is reported [37].

Probe	Sequence
DNA capture probe	5-thiol C6-CAA ACA CCA TTG TCA CAC TGC-3'
miRNA reporter probe	5'-GCA GTG TGA CAA TGG TGT TTG-3'

Table 4.2: Sequencing of the capture and reporter probes used [37].

The experiments are realized in dynamic rage, thanks to the use of a neMESYS syringe pump that provides a flow rate of 0.5 $\mu L/s$.

Finally, the choice of the others parameters is better justified and explained in the Appendix A.

4.2.1 Functionalization of the electrodes: device with single inlet

In this section I report the results obtained by taking the measurement with one device having 8 channels but only one inlet, as represented in Figure 4.3.

The protocol and the conditions of the experiment are the ones already reported (Table 4.1).

The main advantage of this type of device stays in the fact that only one syringe is used, as a consequence the protocol is of faster execution and a less quantity of reagents is used.
However, it is difficult to assure an homogeneous flow rate in every channel and in particular it is impossible to control when it is not. For that reason, I will report only the results obtained for the functionalization, because the ones for the hybridization are of difficult interpretation. In fact, a variation of current of the order of 10-20 nA can be both due to the variation of the flow inside the channel or the sign of hybridization of the capture probes with the reporter probes.

On the other hand, the functionalization always provides changing in current at least of the order of 50 nA respect to the characterization of bare electrodes, that is why even if the flow rate is not homogeneous, the functionalization is visible anyway.

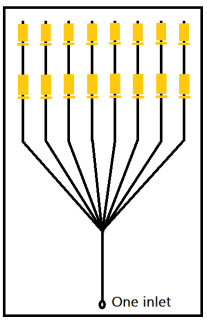

Figure 4.3: Schematic of the device with one inlet and 8 channels. It is possible to observe that every channel has two pairs of electrodes.

Anyway, these measurements are interesting to show the validity of the electrochemical board when 8 measurements are taken at the same time. Figure 4.4 represents the CV measurements taken by the instrumentation, with 8 measurements at the same time, it is possible to observe that the measurements are not noisy and that the electronics components of the board afford this type of experiments.

The measurements are performed before the functionalization of the gold electrodes with the capture probes and after it. The two measurements are then

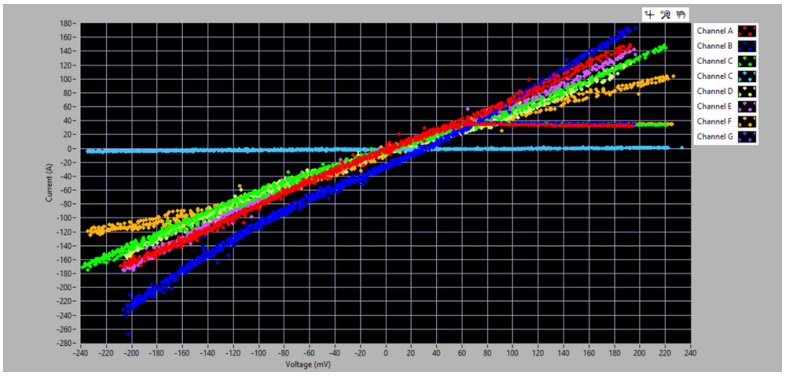

Figure 4.4: Voltammogram from the LabView interface, when 8 measurements are taken at the same time.

compared to check if the SAM has been created.
Each CV measurement is realized in two cycles, such that the autorange gain function (explained in 3.3.3) can take place. Then, the data are saved from the interface, and they are plot and analyzed with the MATLAB program implemented and explained in Data Analysis 3.3.3. Only the second cycle is plotted and analyzed, such that it is possible to have the measurement with the optimized gain.

In Figure 4.5 it is possible to observe the main results obtained before and after functionalization of the electrodes. It is possible to notice that only seven channel measurements are reported, because the channel H was presenting a level of current too low (light blue line in Figure 4.4), maybe due to a damage of the electrodes during the fabrication process. Not the results for all the 16 pairs of the electrodes in the device are reported for the same reason, that's why the choice of showing the result of only one pair of electrodes par channel.

From the Figure it is possible to appreciate the decreasing of the level of current in the case of functionalized electrodes, as expected. The functionalization is also proved by the changing of the shape curve. In table 4.3 are reported the main results for the data analysis, in particular m is the slope [nA/mV] of the central part of the curve on which a linear fit is realized, q is the intercept of the linear fit and abs max and min are respectively the absolute maximum and the absolute minimum of the curves.

It is possible to observe that for the electrodes A,B,C,D and E the differences in maximum or minimum between bare and functionalized electrodes it is of at least 50 nA, and the functionalized electrodes slope of the linear fit is always significantly less respect to the bare electrodes. For what concerns the electrodes F and G, even if the differences in current are not sharply such as in the others electrodes, it is possible to observe the functionalization due to both the changing of the curves shape and the changing of the slope m. In fact, the ratio of m bare over m

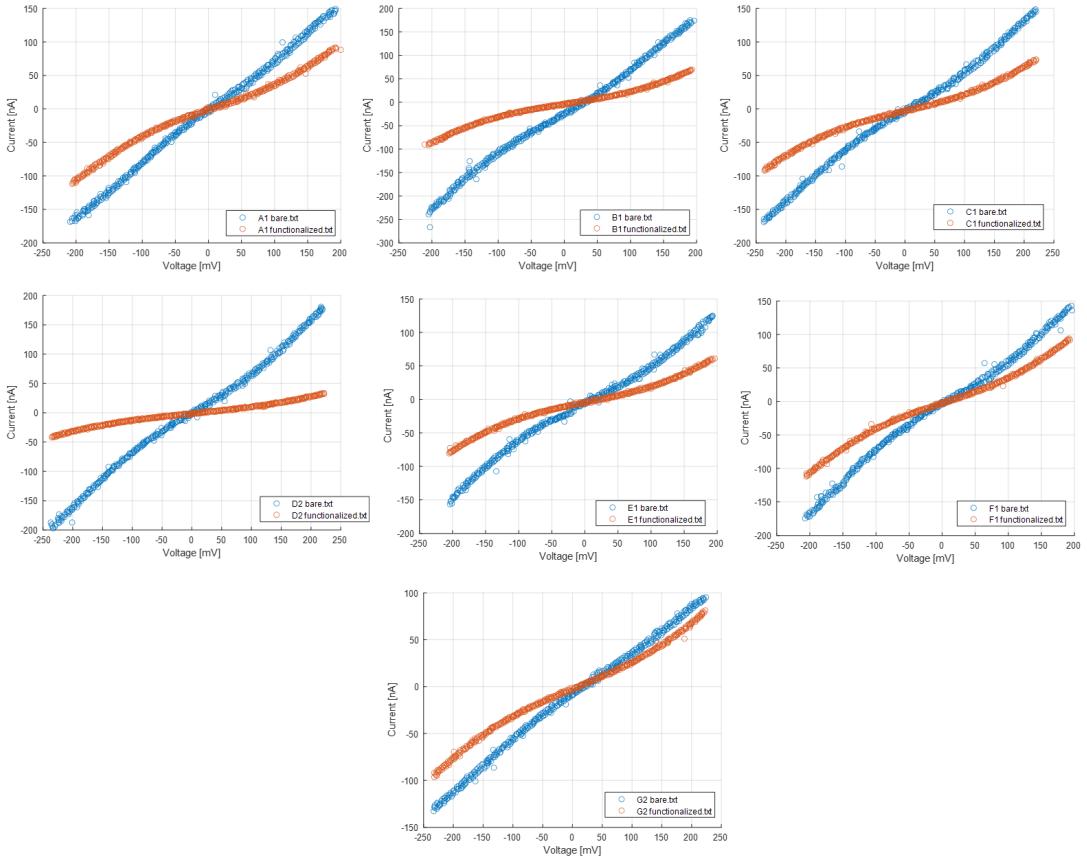

Figure 4.5: CV curves for 7 channels from device in Fig. 4.3.

functionalized is approximately 1.5 for the G electrodes and 1.72 for F electrodes.

As already said, the results obtained for the hybridization will not treated for this device, because they are difficult to interpret. In fact, due to the fact that we are treating data of the order of approximately $10 \div 100$ nA, a little changing of current caused by the changing of the flow rate in the channel, really affects the measurement.

For that reason, the results for the hybridization will be shown the following section, by the use of a different device, but before that, it is interesting to analyze the results from two pairs of electrodes in the same channel.

Comparison same channels different pairs of electrode

In this subsection, the results of the pair of electrodes E1 showed in the previous results, will be compared with the results for the other pairs of electrodes in the same channel, called E2.

Electrodes	m [nA/mV]	q [nA]	abs max [nA]	abs min [nA]
A bare	0.7767	-1.2399	147.4120	-168.3460
A functionalized	0.4177	-1.3445	90.0865	-111.7020
B bare	0.9044	-19.5657	170.9870	-266.5530
B functionalized	0.2989	-3.7218	67.6556	-91.4888
C bare	0.6240	-2.0662	145.6620	-168.7370
C functionalized	0.2799	-2.4719	72.2441	-92.0395
D bare	0.7286	-0.2661	177.1360	-197.1350
D functionalized	0.1266	-0.9250	32.6904	-42.2071
E bare	0.5923	-5.0210	123.2440	-156.5120
E functionalized	0.2649	-4.3428	59.7366	-80.6223
F bare	0.7067	-4.6871	137.3340	-128.9520
F functionalized	0.4107	-2.4121	91.8015	-111.9590
G bare	0.4763	-8.7276	93.9277	-132.6460
G functionalized	0.3166	-2.5062	78.8001	-96.3527

Table 4.3: Data analysis of the measurements plotted on Figure 4.5.

The results are plotted on Figure 4.6 before and after functionalization, and the table 4.4 shows the results. It is possible to observe that even if the curves for the bare electrodes are quite similar, the functionalization did not work in the same way for the two electrochemical cells. This can be due to the fact that more capture probes attached to the E2 electrodes respect to the E1 and this provokes a lower level of current.

This analysis highlights the fact that the data analysis has to be done by comparing relative measurements on the same pair of electrodes during the protocol steps and not absolute values of current from the last step of the protocol.

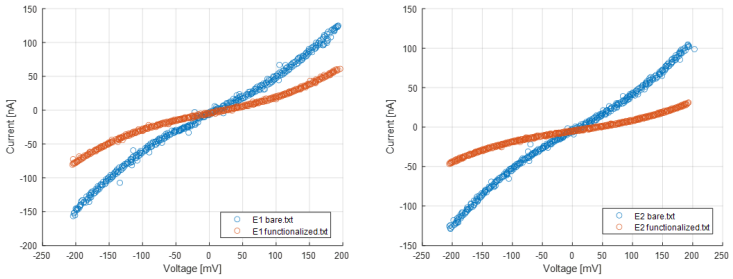

Figure 4.6: CV curves of two electrochemical cells in the same channel, device 4.3.

Electrodes	m [nA/mV]	q [nA]	abs max [nA]	abs min [nA]
E1 bare	0.5923	-5.0210	123.2440	-156.5120
E1 functionalized	0.2649	-4.3428	59.7366	-80.6223
E2 bare	0.4992	-4.8602	102.4620	-128.9520
E2 functionalized	0.1475	-4.6931	29.9197	-46.6425

Table 4.4: Data analysis for CV curves in 4.6.

4.2.2 Functionalization and hybridization: device with 8 inlets

Now that the problematics of the previous device are explained, the experiments are done by the use of a different device. Figure 4.7 shows the device used now, there, 8 different pumps will be needed to perform the measurements on the 8 channels simultaneously.

However, with this type of device it is possible to assure that the flow rate is homogeneous in the 8 channels, and so to correctly interpret the results.

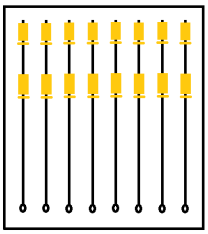

Figure 4.7: Device with separated channels, 8 inlets.

Again, the conditions of the experiment are the one already treated and the protocol is the same, with the difference that three different concentration of reporter probes are tried, starting from the lowest to the highest one.

The concentration of reporter probes used for this experiments are the following ones:

- $T_{36} = 10^{-18}\ \mu g/mL$;
- $T_{33} = 10^{-12}\ \mu g/mL$;
- $T_{30} = 10^{-6}\ \mu g/mL$.

The results are plotted in Figure 4.8 and the data analysis is reported on table 4.5.

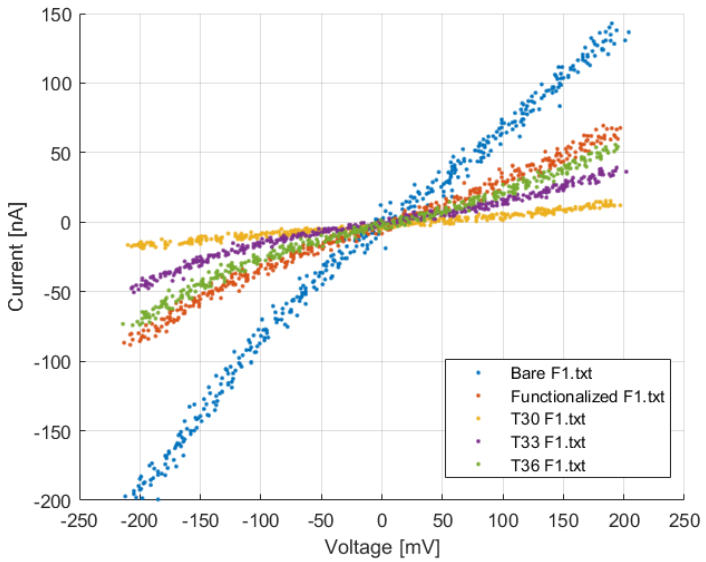

Figure 4.8: CV data from the device showed in Fig. 4.7.

Electrodes	m [nA/mV]	q [nA]	abs max [nA]	abs min [nA]
F1 bare	0.7900	-6.2349	139.9690	-198.0820
F1 functionalized	0.3339	-1.1353	69.3632	-88.2292
F1 T36	0.2568	-1.5815	54.0612	-74.1046
F1 T33	0.1658	0.2129	38.2816	-50.4598
F1 T30	0.0676	-1.6519	15.2468	-18.6062

Table 4.5: Data analysis for CV curves in 4.8.

It is possible to see, as in the previous analysis that the functionalization worked pretty well, in particular, the difference in the absolute maximum before and after functionalization is of the order of 70 nA, while the difference in the absolute minimum is of approximately 110 nA and the slope it is more then halved.

The most interesting results, are the hybridization part, in fact, it is possible to appreciate how, by increasing the concentration of the reporter probes, the current decreases of at least 10−15 nA.

Moreover, in Figure 4.9 it is reported the histogram for the slope fit for each curve represented in the image. In fact this slope is a really interesting parameter because, together with the absolute and minimum values, is the proof that the hybridization worked. It is possible to observe how it gradually decreases with the increasing of the reporter probes concentration. In fact after the functionalization it is more the halved, and by increasing the concentration the ratio between the

slope coefficients goes from 1.3 to 2.4.

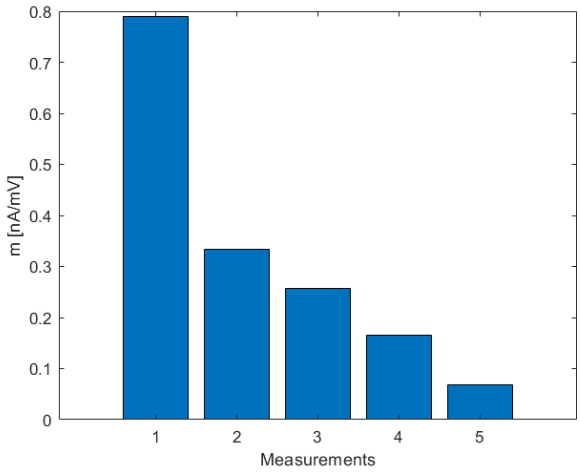

Figure 4.9: Slope parameter fitted for the 5 measurements reported in table 4.5.

These data are really interesting, because they show the validity of the electronic instrumentation, of the use of the hybridization such as a filter and this process as a method of miRNA quantification.

Other interesting measurements are obtained with this same pair of electrodes, the day after. In fact, the deshybridization by the use of flowing water is realized, such that the levels of current reaches almost the values of the functionalized electrodes ($\approx \pm$ 70 nA). Then, the hybridization is again performed, for T36, T33 and T30 concentrations. However, the hybridization for the concentration T33 did not worked, too high current values were obtained, and so it is not plotted in the result of Figure 4.10. On table 4.6, it is possible to see the analyzed data.

Electrodes	m [nA/mV]	q [nA]	abs max [nA]	abs min [nA]
F1 deshybridized	0.3128	1.6075	74.7132	-73.2115
F1 T36	0.2489	-4.0018	45.8041	-64.4824
F1 T30	0.1178	0.5005	25.2931	-37.5783

Table 4.6: Data analysis for CV curves in 4.8.

It is also appreciable that the results are really similar to the ones obtained the day before, with particular interest with the lowest concentration (T30), on which the minimum and maximum values are really close.

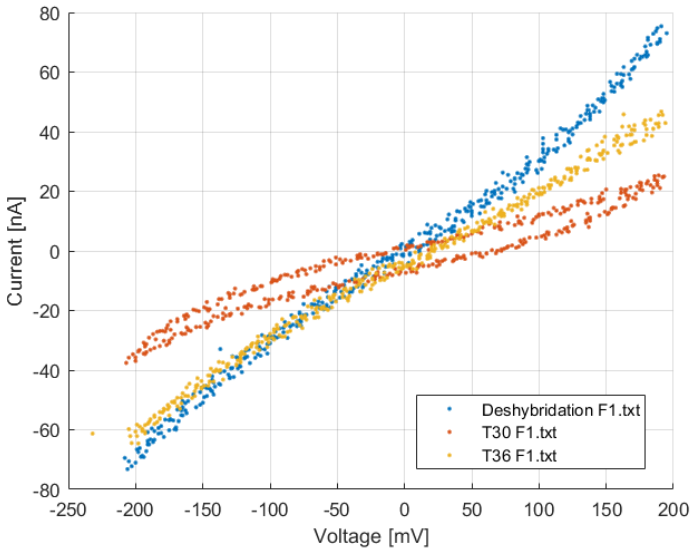

Figure 4.10: CV data after the deshybridization.

4.2.3 Functionalization and hybridization: device with 8 inlets

Another experiment is reported here, again the device used has 8 inlets to guarantee the correct flow rate in each channel, and the conditions of the experiments are the ones already explained.

In Figure 4.11 are reported the results obtained, again the concentration used are T36, T33 and T30, which corresponds to the minimum, the middle and the maximum concentration provided.

Electrodes	m [nA/mV]	q [nA]	abs max [nA]	abs min [nA]
F2 bare	0.9811	-10.9757	158.9170	-230.9780
F2 functionalized	0.3694	-2.8847	71.27972	-100.0590
F2 T36	0.2818	-4.6549	58.1682	-85.7442
F2 T33	0.2404	-2.1322	52.2246	-71.6291
F2 T30	0.1659	-1.5301	35.2499	-39.2066

Table 4.7: Data analysis for CV curves in 4.11.

It is possible to observe that the absolute maximum before and after functionalization differs of approximately 87 nA. While the absolute minimum of 130 nA.

Again, when the different concentrations are inserted the current decreases at

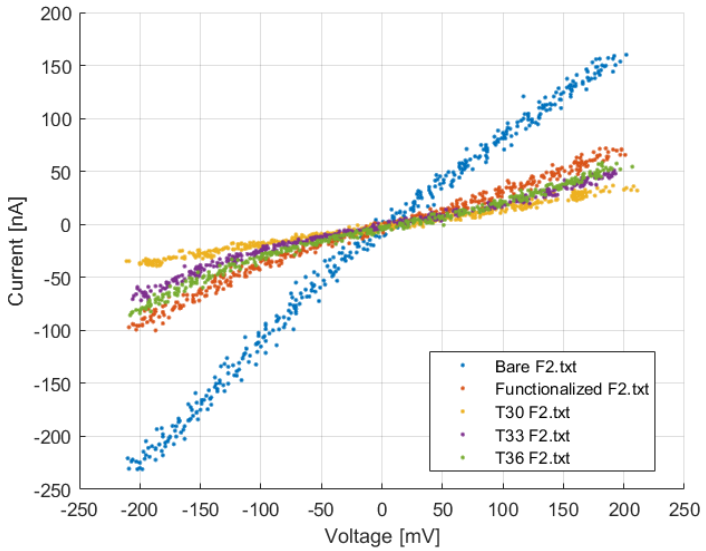

Figure 4.11: CV data from the device showed in Fig. 4.7.

least of $10nA$ per concentration. However, it is not completely clear if the T33 hybridization worked correctly due to the fact that not a relevant difference in the slope and absolute maximum was found respect to the higher concentration T36.

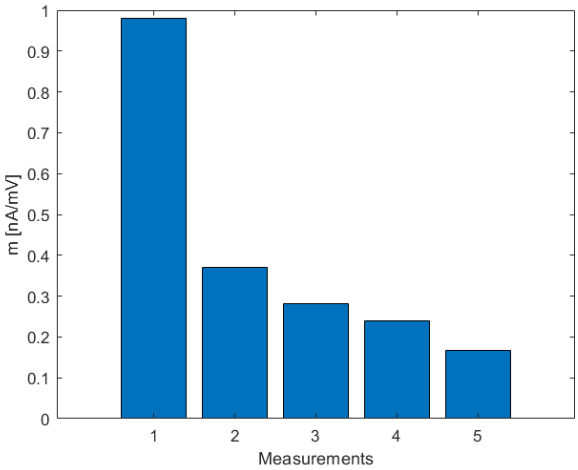

Figure 4.12: Slope parameter fitted for the 5 measurements reported in table 4.7.

Figure 4.12 represents again the histogram of the slope parameter (m) in nA/mV for the five measurements, again it is possible to see that it decreases by increasing the reporter probes concentration, even if in this case the difference is not so relevant

as in the previous measurements (F1), in particular between the concentration T33 and T30.

To conclude, it is possible to see that overall the three steps (characterization, functionalization and hybridization) correctly worked, again, the validity of the device and the electronic instrumentation is confirmed.

4.2.4 Chapter conclusions

In this last chapter I reported the processes exploited for the realization of the Lab on a Chip device and the experiments held on biologic samples.

The main technique for the fabrication of the device is the lithography, in fact two masks are needed: the one to pattern the electrodes component on a glass substrate, and the one to pattern the channels for the PDMS. Then, after the lift-off, these two pieces are manually aligned and bound thanks to the plasma bonding technique.

In the same way, depending on the PDMS pattern chose, it is possible to realize two devices: the device with only one inlet and the one with 8 inlets (Figure 4.3 - 4.7).

The experiments were held with these two devices. In particular, the device with one inlet was useful to prove the validity of the electronics instrumentation when 8 measurements are performed at the same time with the 8 channels of the EC board.

During the experiments, I noticed that the flow in the device with the common inlet was not homogeneous in the 8 channels, and this was confirmed by the measurements taken during the hybridization process, because they were not always coherent. For that reason, only the measurements regarding the characterization and functionalization of the electrodes is reported.

While, thanks to the second device (with 8 inlets) was possible to realize the whole protocol with success. In fact, it was possible to perform the characterization of the electrodes, the functionalization of them with the capture probes and the hybridization with the complementary probes in different concentrations. It was considered a significant hybridization, when the absolute maximum or minimum were decreasing of at least 10-20 nA.

In this way, it was possible to test the whole protocol for what concerns the electrochemistry part and the validity of the EC board is proved.

Chapter 5

Conclusions

During this internship experience I had the opportunity to learn a lot, in fact, despite the lockdown conditions my work was well organized from the beginning thanks to my supervisors.

In the first part of *télétravail* I did the bibliographic work, that was really useful to know and understand the microRNA from the biology point of view.

I also learned a lot about the device and the physical phenomena that it exploits, and I started knowing the electronics under the device. I did the *LTSpice* simulations that result to be really useful to understand the choice of the components, in particular for what concerns the working electrode set up for the electrochemical detection.

After, in laboratory, I had the opportunity to characterize lot of components that I simulated at home, in such way I took confidence with the electronics instrumentation and I compared the result with the theoretical expectation simulated.

One of the main work was the measure of the current for the electrochemistry part, in fact, by characterizing all the stages for the amplification of the current in the working electrode part, I could modify the microcontroller code to read the correct values for the CV measurements from the interface.

Moreover, the implementation of the autorange gain function was an useful tool in order to take the measurement directly with the optimized gain, in this way also the measurement can be performed in less time.

For what concerns the hyperthermia part, the implemented functions to find the resonance frequency and to track the resonance frequency are necessary tools that permit to work at the highest current and so highest magnetic field to heat nanoparticles.

Then, the Full Protocol function implemented to realize both the magnetic hyperthermia and the electrochemistry measurement by inserting all the parameters has been done. In such way, the user will insert all the parameters, so that the full protocol for a maximum of 5 cycle can be realized without the human intervention.

Finally, I did the biologic experiments for the electrochemistry part. What obtained in the experiments can close the whole Electrochemistry part. In fact from the beginning the reason of the work is explained: detect and discriminate between different concentration of a type of miRNA whose dysregulation links to a particular disease. From these experiments, it is possible to prove the validity of the electrochemical protocol,but, in particular, the developed and optimized electrochemical board. In fact, it was possible to link the decreasing of current during a CV measurement to the introduction on the microfluidic device of capture probes, and again, after the introduction of the reporter probes, it was possible to observe a further decreasing of the current due to the hybridization with the complementary targets. Moreover, the link between the increasing of the miRNA concentration in the sample to analyze and the decreasing of the level of current is proved.
All the biologic experiments reported are interesting to prove the good quality of the measurements, the validity of the method and the ability of multiplexing of the electrochemical board.

Further experiments are required to prove the validity of the hyperthermia protocol and instrumentation, and others for what concerns the capture step. Moreover, other implementations and tricks will be introduced in the electrochemistry board and device.

Further research for coupling the electrochemistry technique detection with a thermal sensor will be carried out in a PhD study inside the BioSys team.

Appendix A

EC Parameters Analysis

In this appendix, the different parameters of the EC instrumentation are tested in order to analyze their influence on the measurements. The tests are done on a LOC with Au-Au electrodes already functionalized and the parameters under investigation are: the **integration time**, so at which percentage of the step it is taken the measurement , the **number of samples par point**, so how many measurements are taken for each point (after they are averaged), and the **number of points per cycle** (how many measurements are taken each cycle).

Integration time (%)

The integration time, as represented in Figure A.1, is the exact time at which the measurement is performed during the discretized step voltage, this step voltage it is in general between 100 μV and 10 mV depending on the potentiostats [74]. However, by considering for instance a peak to peak voltage of 0.4V ($\pm$0.2), and by setting 400 points par cycle, this step voltage should be of the order of 2 mV. The current to measure at each point of this step will be not constant, as it is represented in a simplified way in Figure A.2 . For that reason, by playing with this parameter, it is possible to obtain different results.

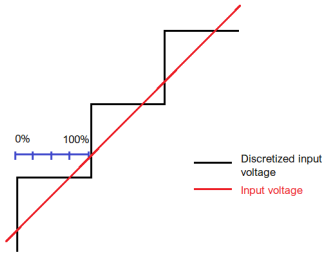

Figure A.1: Integration time (%).

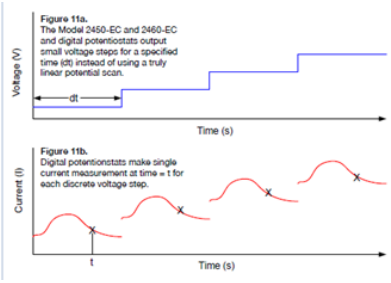

Figure A.2: Discretized voltage (top image), Current shape during the discretized applied voltage (bottom image) [74].

In Figure A.3a, A.3b and A.4a, it is possible to see how the measurement changes by changing the integration time, in fact, at first it is set to 0.01%, then to 0.5% and finally to 1%. It is possible to see that at 0.5% some lower current points start being present, in fact when the measurement is taken for 1% the current measured it is almost the half, sign that we are out of the peak represented in the previous schematic. This is even more clear if we analyze the current changing during the time (Figure A.4b), in particular, in the first cycle the integration time is 0.01%, then to 0.5% and finally to 1%, and the appearance of these lower current points it is more clear at 0.5%.

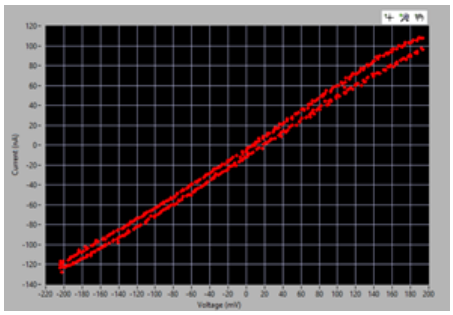

(a) CV measurements for integration time : 0.01%.

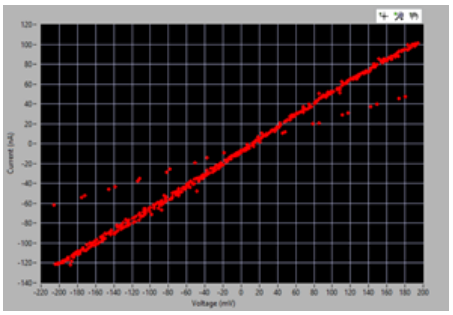

(b) CV measurements for integration time : 0.5%.

Figure A.3: CV measurements by changing the integration time.

It is possible to conclude saying that all the measurements will be preferable taken with a low integration time (maximum limit 0.025%) in order to not to measure the expiring current part . All the measurements reported will be taken with an integration time of 0.01%.

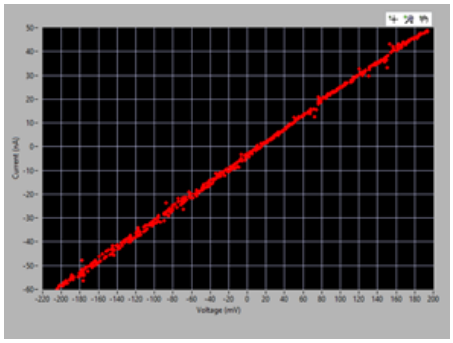

(a) CV measurements for integration time : 1%.

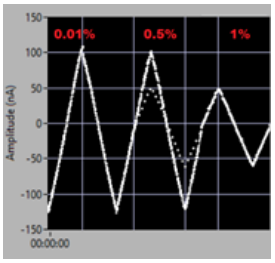

(b) Current vs time: Integration time 0.01%, 0.5%, 1%.

Figure A.4: CV measurements by changing the integration time.

Samples per point

The number of samples per point is the number of points taken for each measurement at the established integration time, then the measurement is averaged. This parameter does not effect at all the measurements as it is possible to observe in Figure A.5a , samples par point equal to 2 , and Figure A.5b , samples par point equal to 4. However, it should not be too high such that the last points are taken at a too high integration time, for that reason, a value between 2 and 4 is recommended.

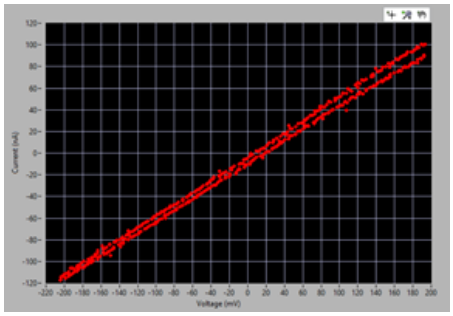

(a) CV measurements with 2 samples per point.

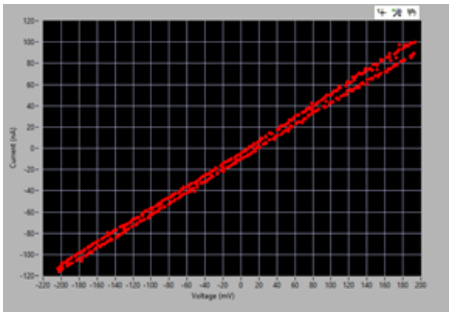

(b) CV measurements with 4 samples per point.

Figure A.5: CV measurements by changing the samples per point.

Number of samples

Finally, the number of samples parameter is analyzed, in particular it represents the number of total points taken for each cycle. In Figure A.6a it is set to 200, in Figure A.6b to 400 and Figure A.6c to 600. It is possible to see that 200 can be an

acceptable number, but by setting it to 400, the measure start being more precise. However, when the number of point is set to 600, the input signal start being more noisy, this is due to the fact that the converter it is not able to perfectly follow the sending signal, as a consequence the output current will be more noisy too. This is even more evident in the input signal showed on Figure A.6e, where 900 points are set for a peak to peak signal of 1 V. For that reason, the recommended number of samples is between 200 (if not extremely precise signal is need) to 500 (for more precise and defined curves).
The same analysis is also done for triangular signal with a peak to peak value of 1 V ($\pm$ 0.5V) and analogue results are found.

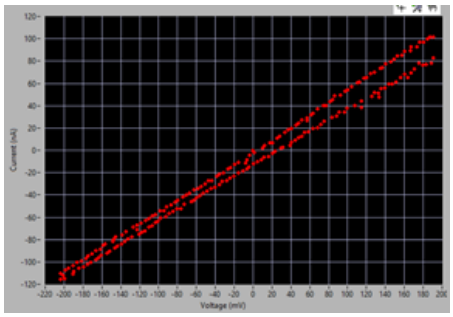

(a) CV measurement for number of samples = 200.

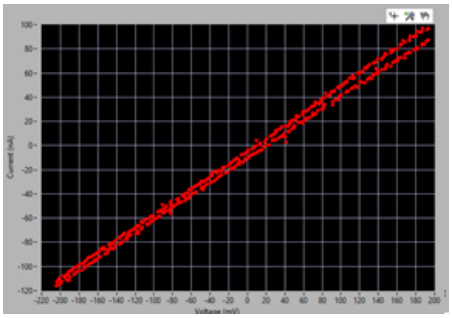

(b) CV measurement for number of samples = 400.

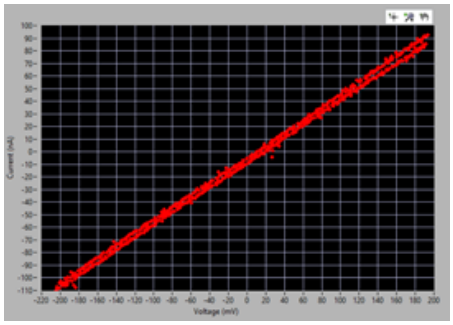

(c) CV measurement for number of samples = 600.

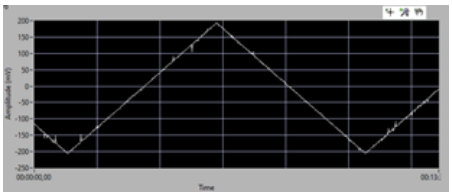

(d) Input signal for number of samples = 600.

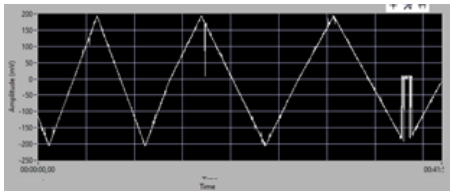

(e) Input signal for number of samples = 900, ($V_{peakpeak}$= 1V).

Figure A.6: CV measurements by changing the numbers of samples.

Bibliography

[1] Marie-Charlotte Horny. «Electrochemistry and magnetic nanoparticles on a microfluidic lab on a chip for medical diagnosis. Detection of microRNA-122». In: *Thèse de Doctorat de l'Université Pierre et Marie Curie* () (cit. on pp. iv, 8, 23, 25, 26, 28, 29, 31, 34).

[2] F.Tonini L.Alberghina. «Biologia. Fondamenti e nuove frontiere». In: *Mondadori Education S.pA., Milano,2005* () (cit. on pp. 2, 3).

[3] «`https://en.wikipedia.org/wiki/RNA`». In: () (cit. on p. 2).

[4] V. Bellotti M. Stoppini. *Biochimica applicata*. EdiSES s.r.l., Napoli, 2012 (cit. on pp. 2, 7).

[5] «`https://en.wikipedia.org/wiki/Nucleic_acid`». In: () (cit. on p. 2).

[6] «The RNA World and the Origins of Life». In: *Garland Science, 2002* () (cit. on p. 3).

[7] «RNA World: a new frontier in biomedical research». In: *European Science Foundation, 2010* () (cit. on p. 3).

[8] Helmenstine Anne Marie. «The 3 Types of RNA and Their Functions». In: *ThoughtCo, 2020, thoughtco.com/types-of-rna-and-their-functions-606386* () (cit. on p. 3).

[9] David P. Bartel. «MicroRNAs: Genomics, Biogenesis, Mechanism, and Function». In: *Cell, 2004* () (cit. on p. 3).

[10] «MicroRNA history: Discovery, recent applications, and next frontiers». In: *Mutation Research, 2011* () (cit. on pp. 3, 4).

[11] «How close are miRNAs from clinical practice? A perspective on the diagnostic and therapeutic market». In: *eJIFCC, 2019* () (cit. on p. 4).

[12] Scott M. Hammond. «An overview of microRNAs». In: *Adv Drug Deliv Rev. , 2015* () (cit. on p. 4).

[13] D. C. Thompson *et alt*. C. E. Condrat. «miRNAs as Biomarkers in Disease: Latest Findings Regarding Their Role in Diagnosis and Prognosis». In: *Cells, MDPI,2020* () (cit. on pp. 4, 5).

[14] «RNA Biomarkers: Diagnostic and Prognostic Potentials and Recent Developments of Electrochemical Biosensors». In: *Small Methods, 2017* () (cit. on pp. 4, 5, 10).

[15] M. A Cortez and G. A. Calin. «MicroRNA identification in plasma and serum». In: *Informa UK, 2009* () (cit. on pp. 4, 5).

[16] «MicroRNA profiling: approaches and considerations». In: *Nat Rev Genet., 2015* () (cit. on p. 4).

[17] «Detection of elevated levels of tumour-associated microRNAs in serum of patients with diffuse large B-cell lymphoma». In: *BJH short report, 2008* () (cit. on pp. 4, 5).

[18] W. You *et alt.* C. Cheng Q. Wang. «MiRNAs as Biomarkers of Myocardial Infarction: A Meta-Analysis». In: *PLOS ONE, 2014* () (cit. on p. 5).

[19] «Lab-on-a-Chip Platforms for Detection of Cardiovascular Disease and Cancer Biomarkers». In: *Sensors, 2017* () (cit. on p. 5).

[20] X. Tian T. Ouyang *et alt.* Z. Liu. «MicroRNA Detection Specificity: Recent Advances and Future Perspective». In: *Anal. Chem., 2019* () (cit. on pp. 6, 11).

[21] «`https://en.wikipedia.org/wiki/Sensitivity_and_specificity`». In: () (cit. on p. 6).

[22] J. Wang T. Tian and X. Zhou. «A review: microRNA detection methods». In: *Royal Soc. of Chemistry, 2014* () (cit. on pp. 6–9, 14).

[23] M. Xu J. Ye *et alt.*. «Research advances in the detection of miRNA». In: *Journal of Pharmaceutical Analysis, 2019* () (cit. on p. 6).

[24] «MicroRNA amplification and detection technologies: opportunities and challenges for point of care diagnostics». In: *Springer Nature, 2018* () (cit. on pp. 6, 7, 9, 14).

[25] K. Ruan W. li. «MicroRNA detection by microarray». In: *Anal. Bioanal. Chem., 2009* () (cit. on p. 6).

[26] «Absolute and Direct MicroRNA Quantification Using DNAGold Nanoparticle Probes». In: *J. Am. Chem. Soc., 2014* () (cit. on p. 7).

[27] Valentina Meli. *Development of a DNA extraction microfluidic lab on a chip device* (cit. on pp. 8, 17, 18).

[28] J. Reiss. «The polymerase chain reaction and its potential role in clinical diagnostics and research». In: () (cit. on p. 8).

[29] A. Man M. U. Kopp A. J. de Mello. «Chemical Amplification: Continuous-Flow PCR on a Chip». In: *Science, 1998* () (cit. on p. 8).

[30] K.J. Livak C.A. Heid J. Stevens *et alt.*. «Real time quantitative PCR». In: *Genome Res.* () (cit. on p. 8).

[31] «`https://en.wikipedia.org/wiki/Real-time_polymerase_chain_reaction`». In: () (cit. on p. 8).

[32] «`https://en.wikipedia.org/wiki/Rolling_circle_replication`». In: () (cit. on p. 9).

[33] X. Tian J. Ye M. Xu *et alt.*. «Research advances in the detection of miRNA». In: *J. Pharm. Anal., 2019* () (cit. on p. 9).

[34] K. Chansiri T. Kaewphinit S. Santiwatanakul. «Quartz crystal microbalance DNA based biosensor for diagnosis: A review». In: *Sensors and Transducers, 2012* () (cit. on p. 10).

[35] D. W. Wegman and S. N. Krylov. «Direct Quantitative Analysis of Multiple miRNAs (DQAMmiR)». In: *Angew. Chem., Int. Ed.,2011* () (cit. on pp. 10–12, 14).

[36] V. Brunetti F. Degliangeli P. Kshirsagar *et alt.*. «Absolute and Direct MicroRNA Quantification Using DNAGold Nanoparticle Probes». In: *Journal of the American Chemical Society, 2014* () (cit. on p. 10).

[37] J. Siaugue *et alt.* M.C. Horny M. Lazerges. «Electrochemical DNA biosensors based on long- range electron transfer: investigating the efficiency of a fluidic channel microelectrode compared to an ultramicroelectrode in a two- electrode setup». In: *Lab on a Chip, Royal Society of Chemistry, 2016* () (cit. on pp. 10, 28, 73, 75).

[38] Y. Zhang and C. Y. Zhang. «Sensitive detection of microRNA with isothermal amplification and a single-quantum-dotbased nanosensor». In: *Anal. Chem., 2012* () (cit. on pp. 11, 14).

[39] L. Zhao *et alt.* W. Yang X. Li. «Quantification of microRNA by gold nanoparticle probes». In: *ScienceDirect,2007* () (cit. on pp. 12, 14).

[40] E. Lopez−Hernandez S. Campuzano R.M. Torrente−Rodriguez *et alt.*. «Magnetobiosensors Based on Viral Protein p19 for MicroRNA Determination in Cancer Cells and Tissues». In: *Angew. Chem., Int. Ed., 2014* () (cit. on pp. 13, 14).

[41] C. Wang *et alt.* Y. Pang. «Fe3O4@Ag magnetic nanoparticles for microRNA capture and duplex-specific nuclease signal amplification based SERS detection in cancer cells». In: *Biosensors and Bioelectronics, 2015* () (cit. on pp. 13, 14).

[42] S. Gupta and S. Ahmed. «Lab-on-Chip Technology: A Review on Design Trends and Future Scope in Biomedical Applications». In: *International Journal of Bio-Science and Bio-Technology 2016* () (cit. on p. 15).

[43] «Encyclopedia of Microfluidics and Nanofluidics». In: *Springer Reference, 2015* () (cit. on pp. 15–17).

[44] S. Haeberlea and R. Zengerle. «Microfluidic platforms for lab-on-a-chip applications». In: *Lab on a Chip, 2007* () (cit. on p. 15).

[45] C. H. Mastrangelo. «DNA ANALYSIS SYSTEMS ON A CHIP.» In: *Center for Integrated Sensors and circuits, Department of Electrical Engineering and Computer Science, University of Michigan* () (cit. on pp. 15–17).

[46] «Development and evaluation of a microdevice for amino acid biomarker detection and analysis on Mars.» In: *Proc Natl Acad Sci USA, 2005* () (cit. on p. 15).

[47] S. N. Brahmasandra *et alt.* M. A. Burns B. N. Johnson. «An Integrated Nanoliter DNA Analysis Device». In: *Science mag, 1998* () (cit. on p. 15).

[48] Lisa R. Volpatti and Ali K. Yetisen. «Commercialization of microfluidic devices». In: *Trends in Biotechnology, CellPress, 2014* () (cit. on p. 16).

[49] «`https://www.grandviewresearch.com/industry-analysis/microfluidics-market`». In: () (cit. on p. 16).

[50] «System Integration: A Major Step toward Lab on a Chip». In: *BioMed Central, 2011* () (cit. on p. 16).

[51] «Microfluidics-based diagnostics of infectious diseases in the developing world». In: *Nature Medicine, 2011* () (cit. on p. 16).

[52] `https://www.elveflow.com/microfluidic-tutorials/microfluidic-reviews-and-t`. «Introduction to lab-on-a-chip 2015 : review, history and future». In: () (cit. on p. 17).

[53] «Lab-on-a-chip or Chip-in-a-lab: Challenges of commercialization lost in translation». In: *Science Direct, 2015* () (cit. on p. 17).

[54] Robert J. Wood. *The Challenge of Manufacturing Between Macro and Micro* (cit. on p. 17).

[55] Athanasios T. Giannitsis. «Microfabrication of biomedical lab-on-chip devices. A review». In: () (cit. on pp. 18, 19).

[56] `https://en.wikipedia.org/wiki/Polydimethylsiloxane`. «PDMS». In: () (cit. on p. 19).

[57] «`https://en.wikipedia.org/wiki/Magnetic_nanoparticles`». In: () (cit. on p. 24).

[58] S.H. Pawar A.B. Salunkhe V.M. Khot. «Magnetic Hyperthermia with Magnetic Nanoparticles: A Status Review». In: *Current topics in medicinal chemistry , 2014* () (cit. on pp. 24–26).

[59] Lise-Marie LACROIX. «Nanoparticules de fer de taille contrôlée pour l'hyperthermie : Synthèse par voie organométallique, caractérisations magnétiques et mesures de puissance dissipée». In: *PhD thesis, Doctorat de l'Université de Toulouse,2008* () (cit. on pp. 24, 25).

[60] J. Overgaard O.S. Nielsen M. Horsman. «A future for hyperthermia in cancer treatment?» In: *European Journal of Cancer, 2001* () (cit. on p. 26).

[61] S. Dutz. «Magnetic Particle Hyperthermia. Biophysical Limitations of a Visionary Tumour Therapy». In: *Journal of Magnetism and Magnetic Materials, 2007* () (cit. on p. 26).

[62] «Impact of magnetic field parameters and iron oxide nanoparticle properties on heat generation for use in magnetic hyperthermia». In: *Journal of Magnetism and Magnetic Materials, 2015* () (cit. on p. 26).

[63] E. S. Rountree N. Elgrishi B. D. McCarthy *et alt.*. «A Practical Beginner's Guide to Cyclic Voltammetry». In: *Journal of ChemicalEducation, 2018* () (cit. on pp. 27, 28, 30, 32, 33).

[64] C. Ho F. Wei P. B. Lillehoj. «DNA Diagnostics: Nanotechnology-Enhanced Electrochemical Detection of Nucleic Acids». In: *Pediatric Research, 2010* () (cit. on pp. 27, 33).

[65] Larry R. Faulkner Allen J. Bard. «ELECTROCHEMICAL METHODS Fundamentals and Applications». In: *JOHN WILEY SONS, INC., 2001* () (cit. on pp. 28–32).

[66] C. Liu D.Jiang G. Xiang et al. «Development of a Cyclic Voltammetry Method for DNA Electrochemical Detection on Microfluidic Gene Chip». In: *International Journal of ELECTROCHEMICAL SCIENCE, 2012* () (cit. on p. 28).

[67] Marco Vergani. «Electronic Instrumentation for Electrochemical Cell Monitoring in Lab-on-Chip Devices». In: *PhD Thesis, Politecnico di Milano, Doctoral Program In Information Engineering* () (cit. on pp. 29, 31, 50).

[68] J. E. B. Randles. «KINETICS OF RAPID ELECTRODE REACTIONS.» In: *Discussions of Farady Society, 1947* () (cit. on p. 32).

[69] «`https://en.wikipedia.org/wiki/LC_circuit`». In: () (cit. on p. 43).

[70] Ron Bertrand. «Online radio and electronics course». In: *`http://www.radioelectronicschool.com/`* () (cit. on p. 43).

[71] P. Ll. Miribel J. P. Villagrasa J. Colomer-Farrarons. «Bioelectronics for Amperometric Biosensors». In: (2013) (cit. on p. 52).

[72] Barry Erhman Tony Wang. «Compensate Transimpedance Amplifiers Intuitively». In: (2005) (cit. on p. 52).

[73] Bonnie Baker. «How to Design Stable Transimpedance Amplifiers for Automotive and Medical Systems». In: (2007) (cit. on p. 53).

[74] Electrochemistry Lab System. «Performing Cyclic Voltammetry Measurements Using Model 2450-EC or 2460-EC». In: () (cit. on pp. 89, 90).